Cell Reports

Report

Ascl1 Balances Neuronal versus Ependymal Fate in the Spinal Cord Central Canal

Graphical Abstract

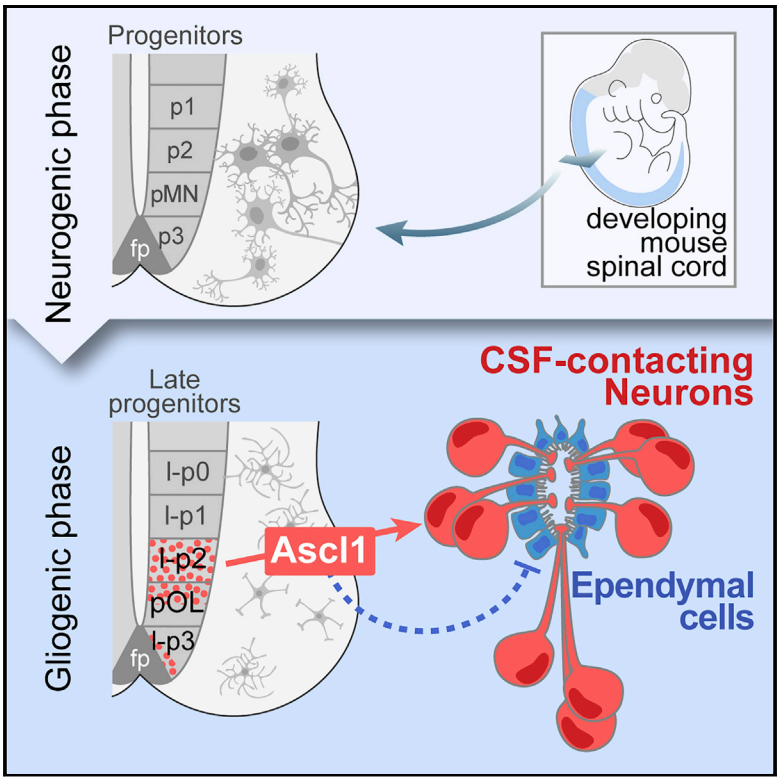

Authors

Daniela J. Di Bella, Abel L. Carcagno, M. Lucía Bartolomeu, ..., Matthias Hammerschmidt, Antonia Marín-Burgin, Guillermo M. Lanuza

Correspondence

glanuza@leloir.org.ar

In Brief

Cerebrospinal fluid-contacting neurons (CSF-cNs) are produced during the gliogenic phase of spinal cord development. Di Bella et al. demonstrate that, in amniotes, CSF-cNs arise from late Ascl1-expressing cells, and this transcription factor controls their development at the expense of ependymal cells. Thus, Ascl1 confers neurogenic potential to late spinal progenitors.

Highlights

- Spinal cord cerebrospinal fluid-contacting neurons (CSF-cNs) are late-born neurons
- CSF-cNs derive from Ascl1-expressing ventral progenitors
- Delayed Ascl1 initiates CSF-cNs differentiation and suppresses ependymogenesis
- Ascl1 controls neuronal and non-neuronal composition of the spinal central canal

Di Bella et al., 2019, Cell Reports *28*, 2264–2274
August 27, 2019
https://doi.org/10.1016/j.celrep.2019.07.087

CellPress

OPEN ACCESS
CellPress

Cell Reports
Report

Ascl1 Balances Neuronal versus Ependymal Fate in the Spinal Cord Central Canal

Daniela J. Di Bella,[1,4] Abel L. Carcagno,[1,4] M. Lucía Bartolomeu,[1] M. Belén Pardi,[2] Heiko Löhr,[3] Nicole Siegel,[1] Matthias Hammerschmidt,[3] Antonia Marín-Burgin,[2] and Guillermo M. Lanuza[1,5,*]

[1]Fundación Instituto Leloir and Consejo Nacional de Investigaciones Científicas y Técnicas (IIBBA-CONICET), Buenos Aires 1405, Argentina
[2]Instituto de Investigación en Biomedicina de Buenos Aires, Partner Institute of the Max Planck Society (IBioBA-CONICET), Buenos Aires, Argentina
[3]Institute of Zoology-Developmental Biology, Center for Molecular Medicine Cologne, Excellence Cluster on Cellular Stress Responses in Aging-Associated Diseases, University of Cologne, Cologne, Germany
[4]These authors contributed equally
[5]Lead Contact
*Correspondence: glanuza@leloir.org.ar
https://doi.org/10.1016/j.celrep.2019.07.087

SUMMARY

Generation of neuronal types at the right time, location, and number is essential for building a functional nervous system. Significant progress has been reached in understanding the mechanisms that govern neuronal diversity. Cerebrospinal fluid-contacting neurons (CSF-cNs), an intriguing spinal cord central canal population, are produced during advanced developmental stages, simultaneous with glial and ependymal cells. It is unknown how CSF-cNs are specified after the neurogenesis-to-gliogenesis switch. Here, we identify delayed Ascl1 expression in mouse spinal progenitors during the gliogenic phase as key in CSF-cN differentiation. With fate mappings and time-controlled deletions, we demonstrate that CSF-cNs derive from Ascl1-expressing cells and that Ascl1 triggers late neurogenesis in the amniote spinal cord. Ascl1 abrogation transforms prospective CSF-cN progenitors into ependymocytes. These results demonstrate that late spinal progenitors have the potential to produce neurons and that Ascl1 initiates CSF-cN differentiation, controlling the precise neuronal and nonneuronal composition of the spinal central canal.

INTRODUCTION

Over the last two decades, substantial advances have been made in deciphering the gene-regulatory programs that command neuronal diversity in the spinal cord and their organization in functional sensory and motor circuits. During development, distinct classes of neurons are produced from progenitors at defined coordinates along the dorso-ventral and anterior-posterior axes of the neural tube. Transcriptional networks translate morphogen signaling into at least 14 cardinal populations of spinal neurons, defined by their origin, gene expression, axon projection, and neurotransmission. These are dorsal dI1-dI6 and dILA/B, ventral V0-V3 interneurons, and motoneurons (Jessell, 2000; Briscoe and Novitch, 2008; Goulding, 2009; Lai et al., 2016; Francius et al., 2013).

Subsequent to the neurogenic phase, which spans until about embryonic day (E) 13 in the mouse spinal cord, the undifferentiated progenitors begin to generate glial and ependymal cells (Rowitch and Kriegstein, 2010). The neurogenesis-to-gliogenesis sequence is accompanied by changes in gene expression that reflect progenitor competence switch (Stolt et al., 2003; Deneen et al., 2006; Rowitch and Kriegstein, 2010). Thus, it was considered that neurons were exclusively generated in the early phases of neural tube development, while later periods were assumed to only produce glial and ependymal cells.

In opposition to this principle, we have identified neurogenic events in the mouse spinal cord taking place during surprisingly advanced stages, simultaneous with the production of astrocytes, oligodendrocytes, and ependymocytes. We have demonstrated that late neurogenesis exclusively produces an intriguing class of spinal cells, the cerebrospinal fluid-contacting neurons (CSF-cNs) (Petracca et al., 2016). CSF-cNs are GABAergic neurons around the central canal interspersed with ependymocytes and tanycytes (Bruni, 1998; Marichal et al., 2012; Stoeckel et al., 2003). They are identified by their peculiar morphology, with a prominent dendritic extension with a wide bulb-like structure in contact with the CSF (Vígh and Vigh-Teichmann, 1971, 1998; Vígh et al., 1983). We have shown that CSF-cNs, which express the transcription factors Gata2 and Gata3, do not belong to any of the cardinal early-born populations of spinal neurons (Petracca et al., 2016).

Despite the high conservation of CSF-cNs among chordates and their discovery almost a century ago (Vígh et al., 2004), their development, characteristics, and functions are just beginning to be unraveled. CSF-cNs in different species selectively express the ion channel Pkd2l1, with mechano- and chemo-sensitivity (Djenoune et al., 2014; Huang et al., 2006; Petracca et al., 2016; Orts-Del'Immagine et al., 2014; Ishimaru et al., 2006; Shimizu et al., 2009). Interestingly, recent studies in lamprey and zebrafish indicate that central canal neurons modulate swimming in response to spinal cord bending and changes in CSF composition or flow (Fidelin et al., 2015; Hubbard et al., 2016; Jalalvand et al., 2016a, 2016b; Orts-Del'Immagine et al., 2016).

The late origin of CSF-cNs seems to be particular to the amniote spinal cord. In mice, rats, and chicks, CSF-cNs are produced only after the finalization of the neurogenic phase (Petracca et al., 2016; Kútna et al., 2014). In contrast, in zebrafish and *Xenopus*, CSF-cNs differentiate together with primary motoneurons and simultaneously or preceding other interneurons (Binor and Heathcote, 2001; Park et al., 2004; Yang et al., 2010; Yeo and Chitnis, 2007). The remarkable late specification of CSF-cNs in the mouse poses the question of which mechanisms are underlying simultaneous neuronal and nonneuronal development after the neurogenic-to-gliogenic switch of spinal precursors.

In this study, we identify that the neuronal potential of late ventral progenitors of the mouse spinal cord relies on the basic helix-loop-helix (bHLH) transcription factor Ascl1. We show that Ascl1 is expressed in progenitors that give rise to central canal neurons. Ascl1 activity during the gliogenic period cell-autonomously triggers neuronal differentiation and ensures the selection of the CSF-cN identity. In addition, we provide strong genetic evidence that Ascl1 controls neuronal versus nonneuronal fate decisions, establishing the balance between ependymocytes and neurons in the amniote spinal cord central canal.

RESULTS

Ascl1 Is Expressed in Ventral Spinal Cord Progenitors during Advanced Embryonic Stages

We hypothesized that late CSF-cN neurogenesis required potent and dedicated transcriptional regulation. As we found that the proneural protein Ascl1 had an expression resembling the CSF-cN pattern, we decided to investigate further. Ascl1 begins to be expressed in the neural tube around E10 with a robust dorsal presence (Helms et al., 2005; Kriks et al., 2005; Wildner et al., 2006) and a spotty ventral expression, mostly limited to the p2 domain (Figures S1A and S1C; Li et al., 2005; Sugimori et al., 2007). At E13.5, corresponding to the neurogenic-to-gliogenic switch, the spatial pattern of Ascl1 remains largely unchanged (Figures S1A–S1D). Double stainings for Ascl1 and transcription factors with dorso-ventral restriction (Figures 1A–1D) show ventral Ascl1$^+$ cells embedded in Nkx6.1$^+$ territories (Figure 1B), dorsal to Olig2 and Nkx2.2 domains (Figures 1C and 1D). Few Ascl1$^+$ cells are in the Olig2$^+$ region (Figure 1C) and at the most ventral Nkx2.2$^+$ p3 domain (Figures 1B–1D).

At E13.5, the dorso-ventral distribution of cells with high Ascl1 levels (Figure 1F) is strikingly similar to the positions where Pkd2l1-expressing neurons start to appear 1 day later, at E14.5 (Figures 1E–1H; Petracca et al., 2016). This correspondence suggests a relationship between Ascl1 and the neurogenic events that generate CSF-cNs.

Central canal neurons are produced at two distinct dorso-ventral regions into two subsets with specific positions around the central canal, electrophysiological properties, morphologies, and functions (Djenoune et al., 2017; Petracca et al., 2016; Park et al., 2004; Yang et al., 2010; Böhm et al., 2016; Hubbard et al., 2016). In the mouse, late p2-pOL (oligodendrocyte progenitor domain) cells produce the CSF-cN′ subset, while the boundary between the p3 domain and the floor plate (fp) generates CSF-cNs″ (Figure 1H; Petracca et al., 2016). Consistent with an association between Ascl1 and both CSF-cNs groups, we found that 97% ± 4% of Ascl1$^+$ cells are positive for Nkx6.1 (Figure 1I), which is present in all CSF-cNs (Orts-Del'Immagine et al., 2014; Petracca et al., 2016). Furthermore, we detected Ascl1 in Foxa2$^+$ cells adjacent to the fp (Figure 1J).

CSF-cNs differentiate from progenitors still mitotically active at E13 and E14 (Petracca et al., 2016). We found that 90% ± 5% of Ascl1-expressing cells incorporated BrdU when applied at E13–E13.5 (Figures 1K and 1N). Additionally, most Ascl1$^+$ cells are labeled with the progenitor marker Sox9 (Figures 1L and 1N) but lack neuronal βIII-tubulin (Figures 1M and 1N).

Central Canal Neurons Derive from Ascl1-Expressing Progenitors

To determine the fate of late Ascl1-expressing cells, we performed lineage tracing. *Ascl1^{CreER}* mice were used with *tdTomato* reporter and induced with tamoxifen (Tam) at E13.75. At E14.5, in addition to labeled dorsal astrocytes (Figure 1O; Vue et al., 2014), ventral Tomato$^+$ cells were at the origin locations of CSF-cNs (Figures 1O, S1E, and S1F, arrowheads). We found Tomato$^+$,Nkx6.1$^+$ cells in the late p2-pOL (Figures S1E and S1G) and Tomato$^+$ cells expressing Foxa2 and Nkx2.2 at the p3-fp interface (Figures S1E, S1H, and S1I), consistent with developing CSF-cNs′ and CSF-cNs″.

Ascl1-derived cells possess the morphology of differentiating CSF-cNs, including their apical process (Figures 1P–1Q, S1G′, and S1I′). Importantly, E14.5 Tomato$^+$ cells express Gata3 and Gata2 (Figures 1R and 1S), while at E16.5, they express Gata2 and Pkd2l1 (Figures S1J–S1L), all molecular signs of the CSF-cN identity. In addition, the administration of three Tam doses (E13.5–E14.25) marked 76% ± 9% of Pkd2l1$^+$ cells at E18.5, while a single Tam induction labeled fewer cells (Figures 1T, 1U, S1M, and S1N). The incomplete labeling of CSF-cNs is likely a consequence of its asynchronous generation (Petracca et al., 2016). Consistently, *Ascl1:GFP* transgenic mice marked the entire Pkd2l1$^+$ population (Figures S1O and S1P).

Ascl1 Is Necessary for CSF-cN Development

Given Ascl1 expression in CSF-cN lineage, we produced *Ascl1* mutants and found that their spinal cords lack Pkd2l1 expression (Figures 2A–2E). Hypomorphic *Ascl1^{neoflox}* mice (Figures S2F–S2J; Andersen et al., 2014) showed fewer Ascl1^{HIGH} cells at E13.5, even in the absence of recombinase, matching a reduced Pkd2l1$^+$ population at E18.5 (Figures 2A–2D and S2A–S2J). Thus, Ascl1 appears to play a fundamental role in instructing CSF-cN identity, and this is common to both CSF-cN′ and CSF-cN″ (Figure 2D).

Next, we found that Ascl1 cannot be replaced by Neurog2, since *Ascl1^{Neurog2}* spinal cords lack Pkd2l1$^+$ neurons (Figures S2K–S2N). Thus, Ascl1 is not merely promoting neurogenesis of late spinal progenitors, but is also specifically required for CSF-cN specification.

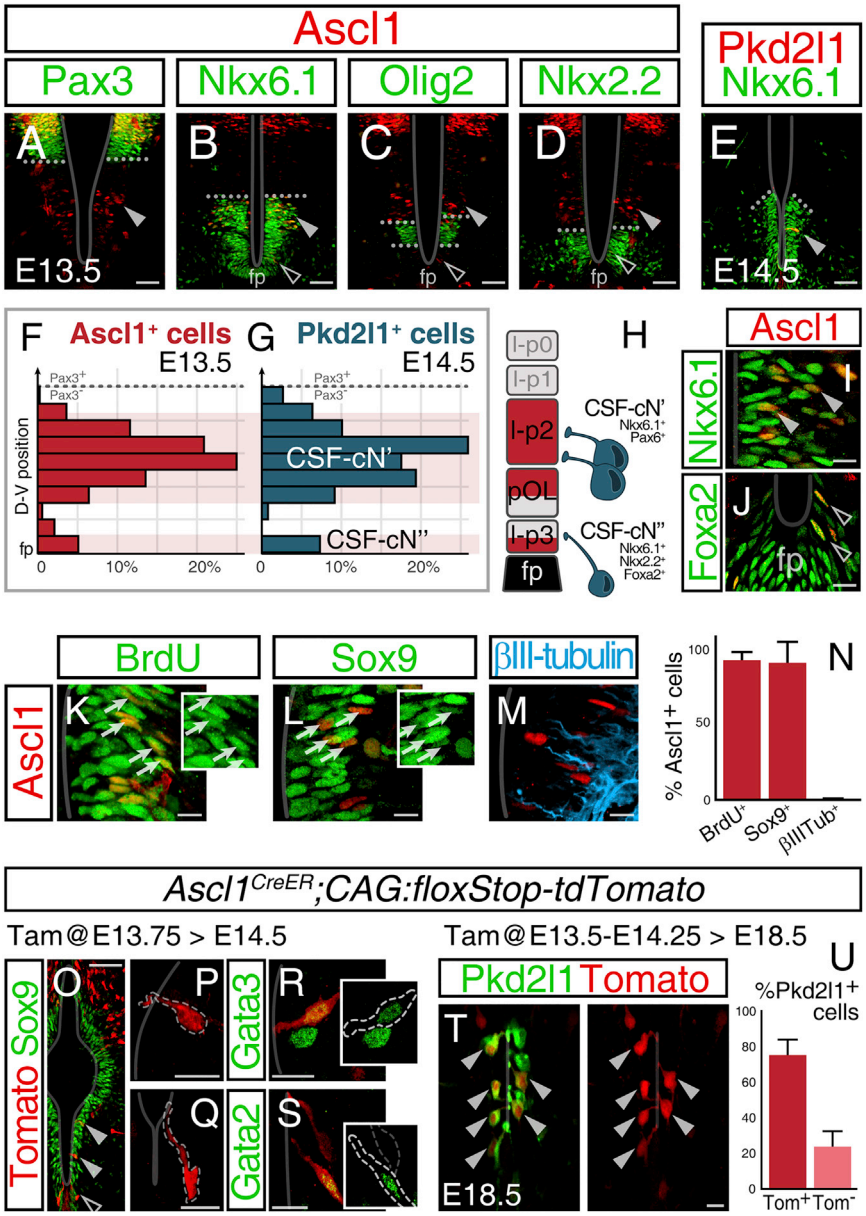

Figure 1. Ascl1 Ventral Spinal Progenitors Give Rise to CSF-cNs

Ascl1 is expressed in the late ventral spinal cord where CSF-cNs are produced.

(A–D) E13.5 mouse neural tube stained for Ascl1 and Pax3 (A), Nkx6.1 (B), Olig2 (C), or Nkx2.2 (D). Arrowheads point to Ascl1$^+$ p2-pOL cells (filled) or p3 cells bordering the fp (empty); n = 3 embryos each.

(E) Staining for Pkd2l1 and Nkx6.1 at E14.5, when CSF-cNs appear.

(F–H) Histograms of dorso-ventral distribution of 484 Ascl1$^+$ cells at E13.5 (F) and 108 Pkd2l1$^+$ neurons at E14.5 (G) (not significantly different, Mann-Whitney test, 6 or 7 embryos) and scheme of the dual origin of CSF-cNs (H).

(I and J) Colocalization of Ascl1 and Nkx6.1 in the p2 area (I) or Foxa2 in the ventral region (J).

(K–N) Ascl1$^+$ cells are late progenitors. Staining for Ascl1 and BrdU (12-h pulses) (K), Sox9 (L), or βIII-tubulin (M) on E13.5 spinal cords and percentage of positive cells (n = 340, 181, 116 cells, 2 or 3 embryos) (N).

(O–S) Late Ascl1$^+$ progenitors give rise to CSF-cNs. E14.5 *Ascl1^{CreER};CAG:floxStop-tdTomato* embryos induced with Tam at E13.75 are stained for Sox9 (O–Q), Gata3 (R), or Gata2 (S).

(R and S) Ventral Tomato cells remain in the ventricular zone and express Gata3 (R) and Gata2 (S).

(T and U) Central canal of E18.5 *Ascl1^{CreER};CAG:floxStop-tdTomato* stained for Pkd2l1, induced with multiple pulses (E13.5–E14.25, n = 292 cells, 4 embryos). Single induction marked 48% ± 19% of CSF-cNs (Tam at E13.75, n = 506 cells, 6 embryos; not shown).

Bars are mean ± SD. Scales are 10 μm, except 40 μm in (A)–(E) and (O).

See also Figure S1.

To determine whether the absence of Pkd2l1 in *Ascl1* mutants truly reflects the lack of CSF-cNs, we evaluated a set of CSF-cN markers. First, we found that βIII-tubulin$^+$ processes are largely absent in the *Ascl1*$^{-/-}$ ependymal area (Figure 2F), contrasting with the projections into the wild-type central canal (Orts-Del'Immagine et al., 2014; Petracca et al., 2016; Stoeckel et al., 2003). Similarly, Gata2, Gata3, and Pkd1l2, partner of Pkd2l1 in CSF-cNs (Petracca et al., 2016; England et al., 2017), are undetectable in the central canal of *Ascl1 KO* (Figures 2G–2I). Neither Nkx6.1^{HIGH} (Figure 2J; Orts-Del'Immagine et al., 2014; Petracca et al., 2016) nor Sox2$^+$/Sox9$^-$ cells (Figure 2K) are found in the *Ascl1*$^{-/-}$ central canal, both of which are characteristic of CSF-cN. Finally, the organized expression of Nkx6.1 and Sox2/9 around the central canal in *Ascl1 KO* mice proves that the absence of CSF-cNs is not due to the lack of the ependymal layer (Figures 2J and 2K).

Furthermore, we analyzed E14.5 embryos, when CSF-cNs normally start to appear, and we rarely found Pkd2l1$^+$, Gata2$^+$, or Gata3$^+$ cells in the *Ascl1* mutant ventricular zone (Figures 2L–2O). The absence of these early post-mitotic markers evidences a failure at the beginning of the CSF-cN differentiation program.

Ascl1 Triggers Neuronal Commitment of Late Progenitors of the Mouse Spinal Cord

Even though CSF-cNs are highly conserved throughout vertebrates (Vígh and Vigh-Teichmann, 1998; Vígh et al., 1977), only in chickens, rats, and mice they arise late during the gliogenic period of development. Despite this clear distinction in developmental timing, CSF-cNs from different organisms share a dual origin and express common identity genes (Djenoune et al., 2014; Petracca et al., 2016; Yang et al., 2010; Andrzejczuk et al., 2018).

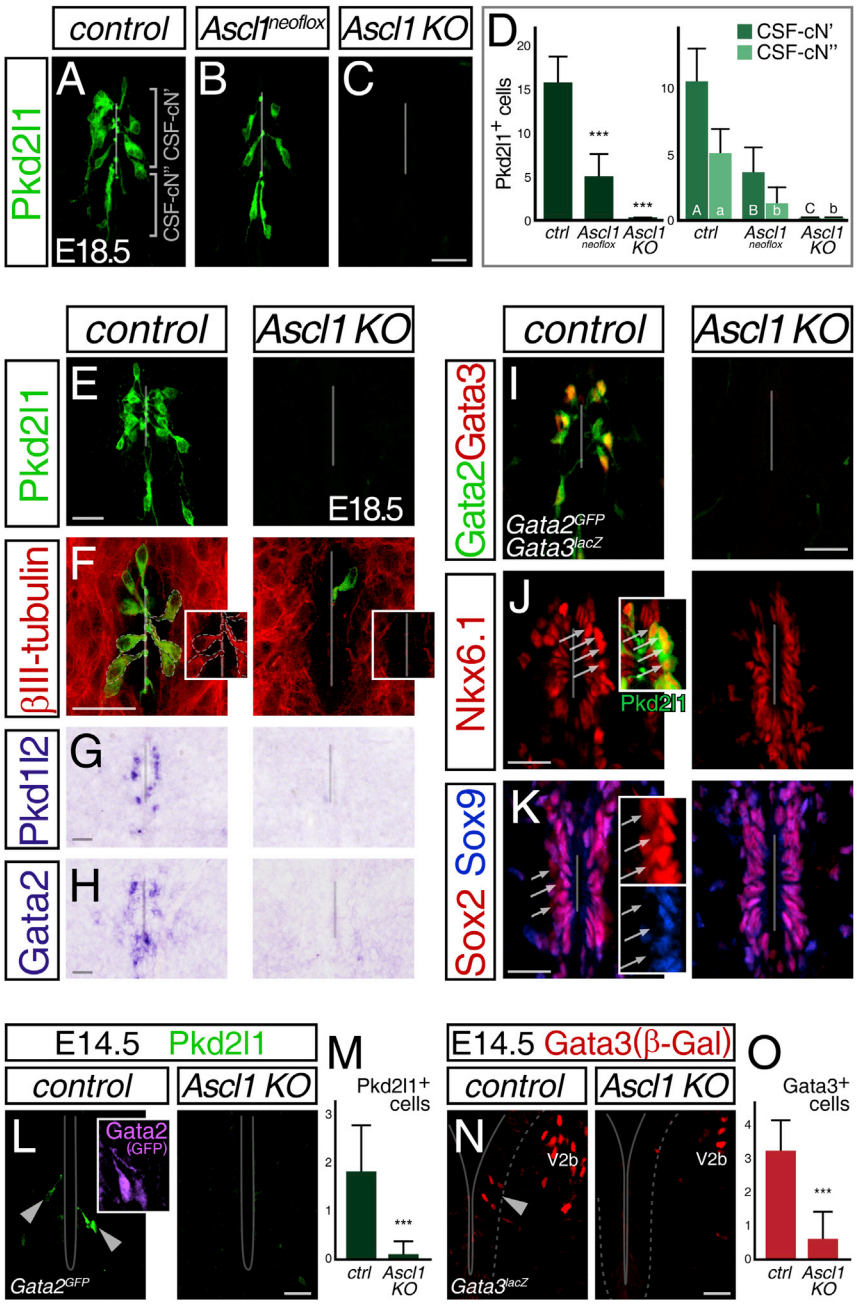

Figure 2. Ascl1 Controls CSF-cN Differentiation

(A–D) Pkd2l1$^+$ neurons depend on Ascl1 expression. Spinal central canal from E18.5 *control* (A), hypomorphic *Ascl1*^{neoflox} (B), and *Ascl1 KO* (C) mice. Number of total Pkd2l1$^+$ neurons (left) or CSF-cN′/CSF-cN″ (right) per section (n = 18–30 sections, 2–4 embryos each) (D). ***p < 0.001, letters indicate significant differences, Kruskal-Wallis with post hoc Dunn's test.

(E–K) *Ascl1* mutants lack CSF-cNs. Staining for Pkd2l1 (E), βIII-tubulin (F), GFP (*Gata2*^{GFP}) and β-Gal (*Gata3*^{lacZ}) (I), Nkx6.1 (J), and Sox2/9 (K), and *in situ* hybridizations for Pkd1l2 (G) and Gata2 (H) in *control* and *Ascl1 KO* E18.5 spinal cord (n = 3–6 embryos each). Arrows point to Nkx6.1^{high} or Sox2$^+$/9$^-$ cells, absent in mutants.

(L–O) CSF-cNs fail to initiate differentiation in *Ascl1* mutants. E14.5 spinal cords stained for Pkd2l1 and GFP (*Gata2*, L) or β-Gal (*Gata3*, N). Positive cells per section in the ventricular zone (arrowheads, M and O, ***p < 0.001, Mann-Whitney test, 10–30 sections, 2 embryos each).

Bars are mean ± SD. Scale bars are 20 μm, 40 μm in (G) and (H).

See also Figure S2.

We asked whether early-born CSF-cNs in non-amniotes are also critically controlled by Ascl1. In zebrafish, the loss or downregulation of *ascl1a* or *ascl1b* had mild effects on the number of CSF-cNs, while the simultaneous downregulation of both paralogs resulted in a reduced Pkd2l1$^+$ population, without losing either CSF-cNs′ or CSF-cNs″ (Figure 3A, ~40% reduction). Thus, in zebrafish, Ascl1 is not an absolute requirement for CSF-cN development. This mechanism contrasts with their specification in the mouse (complete elimination in *Ascl1 KO*), where CSF-cNs arise from unique late neurogenic events through a mechanism fully dependent on Ascl1.

So far, we hypothesized that the activity of Ascl1 in late ventricular cells is crucial for CSF-cN commitment. Nevertheless, their absence in *Ascl1*$^{-/-}$ mice might be due to altered early neurogenesis, changes in proliferation (Castro et al., 2011), or modifications in patterning leading to decreased progenitors. However, in *Ascl1* mutants, we did not find alterations in the differentiation of early V2 neurons or motoneurons (Figures S3A–S3D) or differences in proliferation and density of ventral progenitors at E13.5 (Figures S3E–S3I). Finally, dorso-ventral patterning was not affected in the mutants (Figures S3E and S3G). These experiments indicate that the absence of Ascl1 does not result in defects in the germinative zone that could lead to the lack of CSF-cNs in *Ascl1*$^{-/-}$ embryos.

To rigorously test whether Ascl1 controls the commitment of CSF-cN progenitors at advanced neural tube phases, we designed time window Ascl1 deletions. Previous studies showed that *Foxn4* mutants lack ventral Ascl1 expression at E10–E12 (Figures 3B and 3E; Li et al., 2005; Del Barrio et al., 2007). However, we discovered that by E13.5, Ascl1 is completely recovered in the ventral *Foxn4* null neural tube (Figures 3C and 3E). Interestingly, these mutants develop Pkd2l1$^+$ neurons normally (Figures 3D and 3E), which still depend on Ascl1 (Figures S3J–S3M). Thus, early Ascl1 is unrelated to CSF-cN differentiation, suggesting that the specification of central canal neurons is associated with Ascl1 activity at advanced developmental time

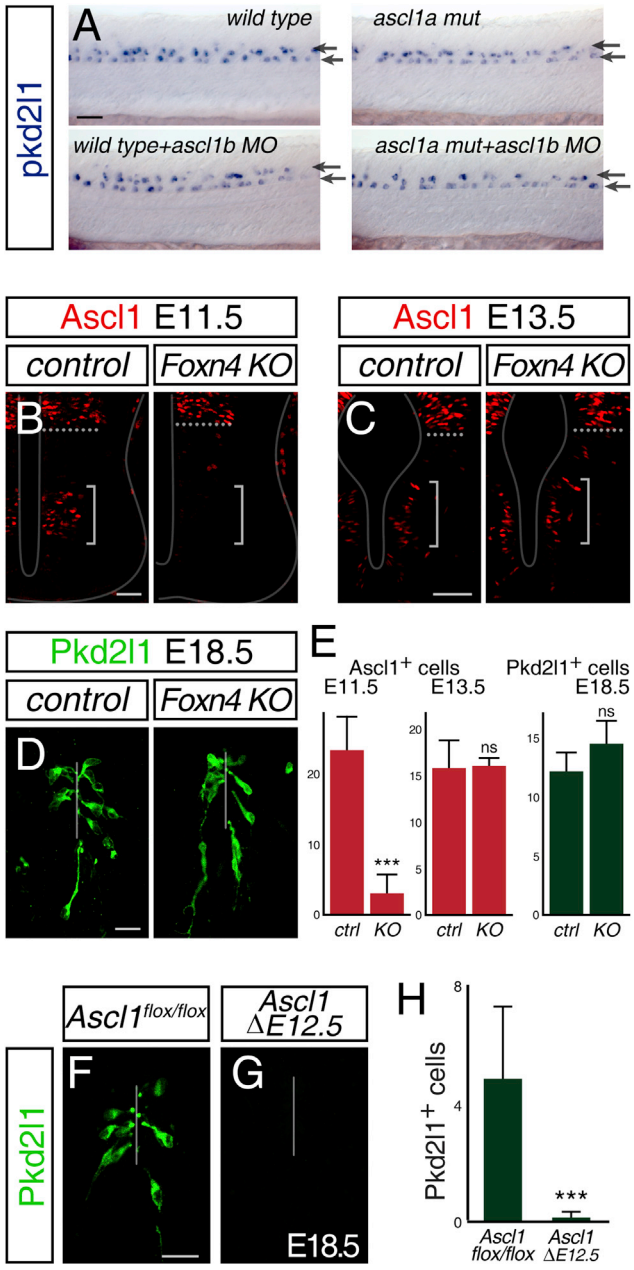

Figure 3. Ascl1 Controls Late Neurogenesis in the Mammalian Ventral Spinal Cord

(A) *ascl1* is not a master regulator of CSF-cN in zebrafish. *pkd2l1* expression in 24 h post-fertilization (hpf) zebrafish (lateral view) *wt or ascl1a* mutants ± *ascl1b* morpholino (MO). *ascl1a* loss and *ascl1b* down-regulation resulted in reduced Pkd2l1$^+$ neurons (*wt* 83 ± 4^a, *ascl1a mut* 69 ± 8^{a,b}, *ascl1b-MO* 71 ± 6^{b,c}, *ascl1a mut+ascl1b-MO* 48 ± 10^c cells; mean ± SD; 10 embryos each), but present and organized in subsets. Letters indicate different groups, $p < 0.05$, Kruskal-Wallis with post hoc Dunn's test.

(B–E) Early Ascl1 is dispensable for CSF-cN production. E11.5 (B) and E13.5 (C) *wt* and *Foxn4 KO* spinal cords are stained for Ascl1; E18.5 for Pkd2l1 (D). Ventral Ascl1$^+$ cells per hemisection, absent in E11.5 *Foxn4*$^{-/-}$, and restored by E13.5 (E) (n = 4–10 sections, 2 embryos each).

points. We generated temporally controlled conditional *Ascl1* knock-outs, using the inducible *CAG:CreER* transgene with the *Ascl1*^{neoflox} allele. Application of Tam at E12.5 to guarantee the elimination of Ascl1 by E13.5 (*Ascl1ΔE12.5*) resulted in the lack of Pkd2l1 expression (Figures 3F–3H), phenocopying *Ascl1* mutants.

In summary, we demonstrate that in the mouse, the delayed second wave of Ascl1 is exclusively responsible for CSF-cN generation, while in zebrafish, the production of CSF-cNs is an early neurogenic event, not fully dependent on Ascl1. We propose that in a gliogenic and ependymogenic context, such as in the mouse, Ascl1 activity is fundamental to initiate CSF-cN differentiation and could then be relevant not only for CSF-cN specification, but also to prevent the acquisition of nonneuronal fates.

Ascl1 Controls Late Neuronal versus Ependymal Fate Decision

To better understand the role of Ascl1 during late spinal cord development, we asked which identity is adopted by prospective CSF-cN progenitors in the absence of Ascl1. We performed fate-mappings using *Ascl1*^{CreER} and *tdTomato*, which, as shown above, mark cells around the central canal, the vast majority Pkd2l1$^+$ neurons (Figures 1T, 1U, and S4A; 74%–100%, low Tam dose for sparse labeling). In *Ascl1* mutants, this protocol rendered an unchanged number of Tomato$^+$ cells in the central canal or in the ventral spinal cord (Figures 4A, 4D, and S4B–S4D).

We first carefully examined the morphology of Tomato$^+$ cells in the ependymal area of *control* and *Ascl1* mutants. As expected, red cells in *controls* have the features of CSF-cNs: a round soma, a process into the central canal lumen, and an axon extending ventrally (Figures 4B, 4C, and S4E). In contrast, Tomato$^+$ *Ascl1*$^{-/-}$ cells possess a wider surface facing the ventricle (Figures 4E–4G and S4F), rarely protrude into the central canal (Figure 4H), and are closer to the ventricle than control cells (Figure S4H). The heterogeneity of labeled cells in *Ascl1 KO* is similar to the morphological diversity of spinal ependymocytes (Figure S4G; Meletis et al., 2008; Bruni, 1998).

These features suggest that prospective CSF-cN progenitors, which fail to acquire neuronal character in the absence of Ascl1, adopt the morphology of central canal ependymocytes. We further analyzed them using a battery of molecular markers. Tomato$^+$ cells in *controls* express Pkd2l1, Gata2, and βIII-tubulin, consistent with the CSF-cN identity, while none in *Ascl1 KO* were positive for these proteins (Figures 4I, 4K, and S4I–S4K). On the contrary, *Ascl1*$^{-/-}$ Tomato$^+$ cells were labeled with antibodies against Foxj1, a ciliation transcription factor expressed after ependymal commitment and absent in murine CSF-cNs (Figure 4J), Sox9, Nfia, Vimentin, and S100β, markers of ependymocytes (Figures 4K and S4L–S4R).

(F–H) Delayed Ascl1 initiates CSF-cNs specification. *Ascl1*^{flox} (F) and *Ascl1-ΔE12.5* (G) E18.5 spinal cords are stained for Pkd2l1 (H) (n = 60 sections, 4 embryos each).

Bars are mean ± SD. ***$p < 0.001$; ns, non-significant; Mann-Whitney test. Scale bars are 40 μm in (B) and (C) and 20 μm in (D), (F), and (G).

See also Figure S3.

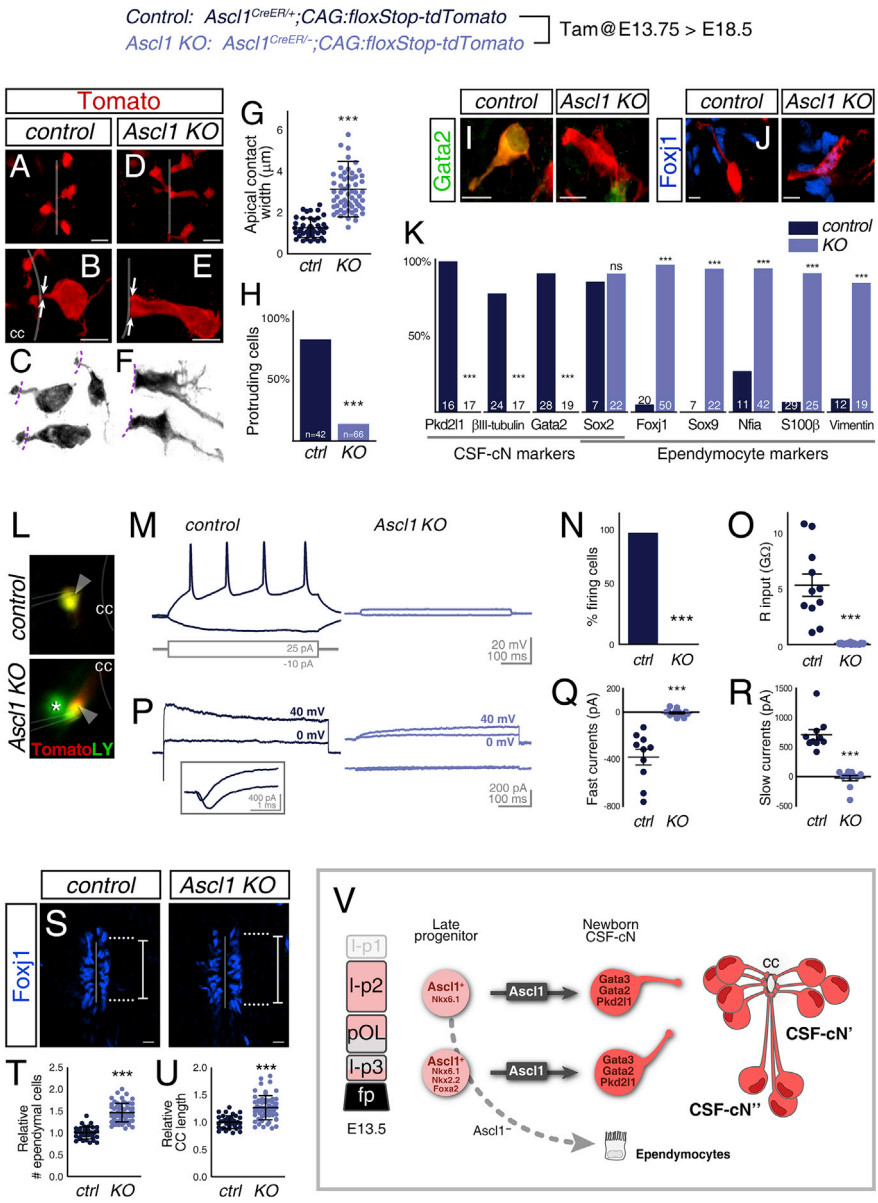

Figure 4. Ascl1 Switches Ependymal to Neuronal Fate of Late Spinal Cord Cells

(A–H) Prospective CSF-cN progenitors acquire ependymocyte morphology in *Ascl1*$^{-/-}$. Labeled cells in E18.5 *control* (A–C) and *Ascl1 KO* (D–F) have distinct morphologies. In *mutants*, Tomato^{+} cells have a wider apical surface (G) and do not protrude in the canal (H). ***p < 0.0001, Mann-Whitney test and Fisher's exact test (n = 40–60 cells each).

(I–K) Labeled mutant cells express ependymal markers. Tomato^{+} cells expressing Gata2 (*GFP*; I) in *control* or Foxj1 (J) in *mutants*. Tomato^{+} cells (%) with CSF-cNs or ependymal markers (K). ***p < 0.001; ns, non-significant; Fisher's exact test. (Number of cells is indicated.)

Distinct membrane properties of labeled cells.

(L) Tomato^{+} cells injected with Lucifer yellow in *KOs* were dye-coupled with neighbors (asterisk, n = 5/7).

(M and N) *Control* labeled cells responded to depolarization with action potentials (25 pA, 500 ms; n = 10/11), but not *mutants* (n = 0/12). ***p < 0.001, Fisher's test.

(O) Mutant cells have lower resistance than *control*s (89 ± 52 macrophage versus 1–10 GΩ; n = 11–13 cells).

(P–R) Evoked currents (P) and quantifications of fast (0–2 ms, 0 mV step; Q) and slow currents (20–70 ms, 40 mV step; n = 10–13 cells; R). ***p < 0.0001, Mann-Whitney test. Results are mean ± SEM.

(S–U) Increased number of ependymocytes in *Ascl1* mutants (T), shown by Foxj1 staining (S), result in an elongated central canal (U). ***p < 0.0001, Mann-Whitney test. Mean ± SD (n = 30 sections, 4 embryos each).

Scale bars are 10 µm in (A), (D), and (S) and 5 µm in (B), (E), (I), and (J). In (G), (T), and (U), lines are mean ± SD.

(V) Summary scheme showing that CSF-cNs arise from two sets of Ascl1^{+} late ventral progenitors in the p2/pOL domain and in the boundary of the p3 domain with the fp. Ascl1 triggers CSF-cN development and controls neuronal versus ependymal fate.

See also Figure S4.

To confirm this neuronal-to-ependymal fate change in *Ascl1* mutants, we recorded the electrophysiological properties of Tomato$^+$ cells by whole-cell patch-clamp. *Control* Tomato$^+$ cells generated action potentials in response to depolarizing steps in current-clamp (Figures 4M and 4N; Petracca et al., 2016; Marichal et al., 2009), while mutant cells were unable to fire (Figures 4M and 4N). In voltage-clamp, *control* cells responded with voltage-dependent, fast inward and slow outward currents, typical of neurons (Figures 4P–4R and S4S). However, Tomato$^+$ cells in mutants showed small currents after changes in potential (Figures 4P–4R and S4S), similar to those described for ependymal cells (Marichal et al., 2012). We also determined that while control cells have a high input resistance, a trait of CSF-cNs (Figures 4O and S4T; Petracca et al., 2016), labeled mutant cells showed strong leakage currents, typical of ependymocytes (Figures 4O and S4T; Bruni, 1998; Marichal et al., 2012). Finally, by including Lucifer yellow in the recording pipette, we found that most mutant Tomato$^+$ cells were dye-coupled with neighboring cells (Figure 4L, asterisk), connections that were not seen in Tomato$^+$ cells of controls (Figure 4L) and that reflect gap junctions between ependymal cells (Bruni, 1998; Marichal et al., 2012).

Altogether, our morphological, molecular, and electrophysiological characterization indicates that late progenitors that normally produce CSF-cNs become ependymocytes of the central canal when missing Ascl1. Consistent with a neuronal-to-ependymal fate transformation, we found that the spinal cord of perinatal *Ascl1* mutants possesses an increased number of ependymocytes in the lateral walls of the central canal (Figures 4S and 4T), resulting in an enlarged canal compared to control spinal cords (Figure 4U).

DISCUSSION

This study demonstrates that neurogenesis during advanced developmental stages of the mouse spinal cord selectively produces CSF-cNs and is strictly dependent on Ascl1. Ventral progenitor cells with delayed Ascl1 expression generate central canal neurons, while the rest of the ventricular zone produces astrocytes, oligodendrocytes, and ependymocytes. We provide compelling evidence that Ascl1 is a key player in the neuronal CSF-cN commitment of late progenitors, controlling the proportion of neurons and nonneuronal cells lining the central canal.

Ascl1 Triggers Late Neurogenesis in the Mouse Spinal Cord

In amniotes, spinal central canal neurons are produced when neurogenesis is largely suppressed and progenitors are massively committed to glial and ependymal fates (Petracca et al., 2016; Rowitch and Kriegstein, 2010). We show that Ascl1 is expressed in a discrete group of late ventral progenitors at dorso-ventral positions matching CSF-cN location and preceding CSF-cN birth. Although Ascl1 is also present earlier in ventral p2 and p3 precursors (Li et al., 2005; Del Barrio et al., 2007; Peng et al., 2007; Sugimori et al., 2007), our experiments indicate that the deferred second wave of Ascl1 is independent of early V2-related Ascl1 expression and linked to the differentiation of CSF-cNs. First, the proper generation of CSF-cNs in *Foxn4* mutants takes place despite the absence of the first round of Ascl1 expression. Second, genetic labeling of the second wave of Ascl1 expression (~E13.5–E14.5) specifically marks central canal neurons. Third, time-controlled deletion of Ascl1 during late stages abrogates CSF-cN neurogenesis.

Our experiments show that *Ascl1* mutant mice are devoid of CSF-cNs, in an expression level-dependent manner. Thus, high levels of Ascl1 activate neurogenesis during the gliogenic phase of the neural tube and initiate CSF-cN specification programs. These findings are in line with Ascl1 being a central player in neuronal commitment (Casarosa et al., 1999; Castro et al., 2011; Raposo et al., 2015) and its role in assigning specific neuronal identities (Parras et al., 2002; Wildner et al., 2006; Helms et al., 2005; Pattyn et al., 2004; Borromeo et al., 2014).

Ascl1 Restricts Ependymal Fate in Prospective CSF-cN Progenitors

Central canal neurons develop from ventral domains that also give rise to vA2-vA3 astrocytes (Hochstim et al., 2008; Tsai et al., 2012), oligodendrocytes (Zhou and Anderson, 2002; Lu et al., 2002), and ependymocytes (Yu et al., 2013; Fu et al., 2003). Our fate mappings show that when neurogenesis is impaired by Ascl1 absence, CSF-cN precursors are converted into ependymal cells lining the central canal. Transfated cells appear to be indistinguishable from non-labeled ependymocytes, with mural apical surface, gap junctions, selective markers, and characteristic membrane properties (Alfaro-Cervello et al., 2012; Bruni, 1998; Marichal et al., 2009).

These results strongly suggest that CSF-cNs are produced from progenitors with cryptic bipotency to generate neurons and ependymal cells and that Ascl1 triggers neuronal commitment. We propose that Ascl1 is crucial to suppress the dedicated program that converts the remaining ventricular cells into ependymocytes (Shimada et al., 2017; Jacquet et al., 2009; Kyrousi et al., 2015).

The role of Ascl1 in CSF-cN differentiation seems unusual compared to the majority of Ascl1 functions, involved in binary decisions between neuronal subtypes (Casarosa et al., 1999; Mizuguchi et al., 2006; Wildner et al., 2006). Interestingly, in the late spinal cord, Ascl1 switches between simultaneously produced neuronal and nonneuronal fates. This is reminiscent of the role of Ascl1 in Schwann cell precursors, where it drives parasympathetic neurons instead of glial differentiation (Dyachuk et al., 2014). Altogether, this proves the extraordinary capacity of Ascl1 to initiate neurogenesis even after commitment toward glial or ependymal fates, and it is consistent with the use of Ascl1 in forced neuronal transformations (Arlotta and Berninger, 2014; Karow et al., 2012; Vierbuchen et al., 2010).

Ascl1 Requirement for CSF-cN Differentiation in Amniotes versus Non-amniotes

Among vertebrate species, there are striking differences in the timing of central canal neurons. In amniotes, such as mice, rats, and chickens, CSF-cNs are produced at advanced stages during the gliogenic phase (Petracca et al., 2016; Kútna et al., 2014) and after interneurons and motoneurons (Rowitch and Kriegstein, 2010). In opposition, non-amniotic vertebrates, like

zebrafish and *Xenopus*, generate CSF-cNs during early development, before or along with the rest of the spinal neurons (Binor and Heathcote, 2001; Shin et al., 2007; Dale et al., 1987b; Yeo and Chitnis, 2007; Huang et al., 2012; Yang et al., 2010; Andrzejczuk et al., 2018). Studies in the lamprey strongly suggest that CSF-cNs are born early during the embryonic and prolarval stages (Meléndez-Ferro et al., 2003). Given that lamprey represents the most ancient group of vertebrates, this heterochrony suggests a post-displacement in the genesis of CSF-cNs in amniotes, relative to the common ancestor (Smith, 2003; McKinney and McNamara, 1991), and may reflect morphogenetic, physical, or phyletic constraints or changes in the selection pressures associated with the role of CSF-cNs in larval swimming (Smith, 2003; Fidelin et al., 2015).

Despite *ascl1* being involved in zebrafish early-born CSF-cN development, it is not the main regulator, as they are still produced upon *ascl1* downregulation. The partial reduction of CSF-cN in *ascl1*-deficient zebrafish is markedly different to the complete loss in mouse *Ascl1 KOs*. The decrease observed in zebrafish might result from altered notch signaling influencing CSF-cN genesis (Shin et al., 2007; Huang et al., 2012), while their differentiation relies on bHLH proteins of the Tal family (Yang et al., 2010; Andrzejczuk et al., 2018). We propose that concurrently with the delay in the developmental timing of central canal neurons along vertebrate evolution, Ascl1 was re-purposed in the gene network that drives late CSF-cN production in amniotes when progenitors are broadly committed to nonneuronal cells.

The Development of Two Subpopulations of CSF-cNs

It is interesting that two distinct lineages, from non-neighboring progenitor regions, converge to produce central canal neurons. The dual source of CSF-cN′ (p2 and pOL) and CSF-cN″ (p3 bordering the fp) contrasts with all other classes of spinal neurons, where subtypes are ontogenetically related and arise from common progenitors (Stam et al., 2012; Bikoff et al., 2016; Goulding, 2009; Delile et al., 2019; Hayashi et al., 2018). Regardless of their domain of origin—either p2-pOL or the tip of p3—the differentiation of central canal neurons in the mouse converge on the activation of Ascl1 to initiate the specification of both clusters (Figure 4V).

The double origin could be crucial for their extended dorsoventral distribution and/or the production of functionally distinct subtypes. Studies in zebrafish and lamprey begin to uncover CSF-cNs' functions and suggest that they constitute a local sensory motor loop to modulate posture during rapid movement (Fidelin et al., 2015; Hubbard et al., 2016; Böhm et al., 2016; Jalalvand et al., 2016a, 2016b). These studies also exposed that dorsal and ventral CSF-cNs differ in neuromodulators, apical and axonal extensions, and intraspinal postsynaptic targets (Böhm et al., 2016; Hubbard et al., 2016; Djenoune et al., 2017). Additionally, CSF-cNs′ respond to horizontal bending, whereas CSF-cNs″ appear to react to longitudinal larval contractions.

In the mouse, CSF-cN′ and CSF-cN″ also have morphological differences and distinctive properties (Petracca et al., 2016), suggesting central canal neurons with separate developmental origins are distinct subtypes that might play specific functions in spinal circuits. While mechanical feedback from spinal bending can provide important information during swimming, the role of central canal neurons in mammals is intriguing. Their presence in every chordate species studied (Vígh et al., 1977, 1983, 2004; Dale et al., 1987a; Barber et al., 1982; Jalalvand et al., 2014; Djenoune et al., 2014) suggests conserved functions. Nevertheless, to what extent bending activation of CSF-cNs plays a role in walking, and whether CSF-cNs respond exclusively to other sensing modalities, remains to be investigated.

In summary, we identified that the transcription factor Ascl1 is key in promoting neuron production after the neurogenic-to-gliogenic switch in the mouse spinal cord. Understanding cell fate mechanisms of late multipotential spinal precursors will be important to manipulate neuronal, glial, or ependymal choices in repair strategies through the reactivation of developmental programs. This study demonstrates that Ascl1 is at the top of the CSF-cN differentiation program, triggering neuronal commitment of cells also capable of producing ependymocytes (Figure 4V). The identification of Ascl1 is an important step in understanding how the intriguing CSF-cNs are specified, and how the neuronal and nonneuronal composition of the central canal is properly balanced.

STAR★METHODS

Detailed methods are provided in the online version of this paper and include the following:

- KEY RESOURCES TABLE
- LEAD CONTACT AND MATERIALS AVAILABILITY
- EXPERIMENTAL MODEL AND SUBJECT DETAILS
  - Mice
  - Zebrafish
- METHOD DETAILS
  - Animals
  - Immunohistochemistry
  - *In situ* hybridization
  - Acute Spinal Cord Slice Recordings
  - Imaging
- QUANTIFICATION AND STATISTICAL ANALYSIS
- DATA AND CODE AVAILABILITY

SUPPLEMENTAL INFORMATION

Supplemental Information can be found online at https://doi.org/10.1016/j.celrep.2019.07.087.

ACKNOWLEDGMENTS

This work was supported by the Agencia Nacional de Promoción Científica y Tecnológica of Argentina PICT2014-1821 and PICT2017-0297 to G.M.L. and PICT2014-3167 to A.L.C. and by the International Society for Neurochemistry (CAEN-ISN) to A.L.C. We thank Micaela Sartoretti, Luciano Brum, Carla Campetella, and Alejandro Schinder for comments and discussions. We thank Jane Johnson, Francois Guillemot, Martyn Goulding, Doug Engel, Mengqing Xiang, and Magdalena Götz for mouse strains and Charles Zuker, Chris Kintner, Kamal Sharma, Javier Ramos, Fernando Pitossi, Sam Pfaff, and Lorena Rela for antibodies or probes.

AUTHOR CONTRIBUTIONS

D.J.D.B., A.L.C., and G.M.L. performed most experiments, analyzed results, and wrote the manuscript. M.L.B. and N.S. performed additional experiments, M.B.P. and A.M.-B. contributed to the electrophysiology, H.L. and M.H. contributed to the zebrafish experiment, and G.M.L. designed the research.

DECLARATION OF INTERESTS

The authors declare no competing interests.

Received: April 2, 2019
Revised: June 7, 2019
Accepted: July 23, 2019
Published: August 27, 2019

REFERENCES

Alfaro-Cervello, C., Soriano-Navarro, M., Mirzadeh, Z., Alvarez-Buylla, A., and Garcia-Verdugo, J.M. (2012). Biciliated ependymal cell proliferation contributes to spinal cord growth. J. Comp. Neurol. *520*, 3528–3552.

Andersen, J., Urbán, N., Achimastou, A., Ito, A., Simic, M., Ullom, K., Martynoga, B., Lebel, M., Göritz, C., Frisén, J., et al. (2014). A transcriptional mechanism integrating inputs from extracellular signals to activate hippocampal stem cells. Neuron *83*, 1085–1097.

Andrzejczuk, L.A., Banerjee, S., England, S.J., Voufo, C., Kamara, K., and Lewis, K.E. (2018). Tal1, Gata2a, and Gata3 Have Distinct Functions in the Development of V2b and Cerebrospinal Fluid-Contacting KA Spinal Neurons. Front. Neurosci. *12*, 170.

Arlotta, P., and Berninger, B. (2014). Brains in metamorphosis: reprogramming cell identity within the central nervous system. Curr. Opin. Neurobiol. *27*, 208–214.

Barber, R.P., Vaughn, J.E., and Roberts, E. (1982). The cytoarchitecture of GABAergic neurons in rat spinal cord. Brain Res. *238*, 305–328.

Bikoff, J.B., Gabitto, M.I., Rivard, A.F., Drobac, E., Machado, T.A., Miri, A., Brenner-Morton, S., Famojure, E., Diaz, C., Alvarez, F.J., et al. (2016). Spinal Inhibitory Interneuron Diversity Delineates Variant Motor Microcircuits. Cell *165*, 207–219.

Binor, E., and Heathcote, R.D. (2001). Development of GABA-immunoreactive neuron patterning in the spinal cord. J. Comp. Neurol. *438*, 1–11.

Böhm, U.L., Prendergast, A., Djenoune, L., Nunes Figueiredo, S., Gomez, J., Stokes, C., Kaiser, S., Suster, M., Kawakami, K., Charpentier, M., et al. (2016). CSF-contacting neurons regulate locomotion by relaying mechanical stimuli to spinal circuits. Nat. Commun. *7*, 10866.

Borromeo, M.D., Meredith, D.M., Castro, D.S., Chang, J.C., Tung, K.C., Guillemot, F., and Johnson, J.E. (2014). A transcription factor network specifying inhibitory versus excitatory neurons in the dorsal spinal cord. Development *141*, 2803–2812.

Briscoe, J., and Novitch, B.G. (2008). Regulatory pathways linking progenitor patterning, cell fates and neurogenesis in the ventral neural tube. Philos. Trans. R. Soc. Lond. B Biol. Sci. *363*, 57–70.

Bruni, J.E. (1998). Ependymal development, proliferation, and functions: a review. Microsc. Res. Tech. *41*, 2–13.

Carcagno, A.L., Di Bella, D.J., Goulding, M., Guillemot, F., and Lanuza, G.M. (2014). Neurogenin3 restricts serotonergic neuron differentiation to the hindbrain. J. Neurosci. *34*, 15223–15233.

Casarosa, S., Fode, C., and Guillemot, F. (1999). Mash1 regulates neurogenesis in the ventral telencephalon. Development *126*, 525–534.

Castro, D.S., Martynoga, B., Parras, C., Ramesh, V., Pacary, E., Johnston, C., Drechsel, D., Lebel-Potter, M., Garcia, L.G., Hunt, C., et al. (2011). A novel function of the proneural factor Ascl1 in progenitor proliferation identified by genome-wide characterization of its targets. Genes Dev. *25*, 930–945.

Dale, N., Roberts, A., Ottersen, O.P., and Storm-Mathisen, J. (1987a). The development of a population of spinal cord neurons and their axonal projections revealed by GABA immunocytochemistry in frog embryos. Proc. R. Soc. Lond. B Biol. Sci. *232*, 205–215.

Dale, N., Roberts, A., Ottersen, O.P., and Storm-Mathisen, J. (1987b). The morphology and distribution of 'Kolmer-Agduhr cells', a class of cerebrospinal-fluid-contacting neurons revealed in the frog embryo spinal cord by GABA immunocytochemistry. Proc. R. Soc. Lond. B Biol. Sci. *232*, 193–203.

Del Barrio, M.G., Taveira-Marques, R., Muroyama, Y., Yuk, D.I., Li, S., Wines-Samuelson, M., Shen, J., Smith, H.K., Xiang, M., Rowitch, D., and Richardson, W.D. (2007). A regulatory network involving Foxn4, Mash1 and delta-like 4/Notch1 generates V2a and V2b spinal interneurons from a common progenitor pool. Development *134*, 3427–3436.

Delile, J., Rayon, T., Melchionda, M., Edwards, A., Briscoe, J., and Sagner, A. (2019). Single cell transcriptomics reveals spatial and temporal dynamics of gene expression in the developing mouse spinal cord. Development *146*, dev173807.

Deneen, B., Ho, R., Lukaszewicz, A., Hochstim, C.J., Gronostajski, R.M., and Anderson, D.J. (2006). The transcription factor NFIA controls the onset of gliogenesis in the developing spinal cord. Neuron *52*, 953–968.

Djenoune, L., Khabou, H., Joubert, F., Quan, F.B., Nunes Figueiredo, S., Bodineau, L., Del Bene, F., Burcklé, C., Tostivint, H., and Wyart, C. (2014). Investigation of spinal cerebrospinal fluid-contacting neurons expressing PKD2L1: evidence for a conserved system from fish to primates. Front. Neuroanat. *8*, 26.

Djenoune, L., Desban, L., Gomez, J., Sternberg, J.R., Prendergast, A., Langui, D., Quan, F.B., Marnas, H., Auer, T.O., Rio, J.P., et al. (2017). The dual developmental origin of spinal cerebrospinal fluid-contacting neurons gives rise to distinct functional subtypes. Sci. Rep. *7*, 719.

Dyachuk, V., Furlan, A., Shahidi, M.K., Giovenco, M., Kaukua, N., Konstantinidou, C., Pachnis, V., Memic, F., Marklund, U., Müller, T., et al. (2014). Neurodevelopment. Parasympathetic neurons originate from nerve-associated peripheral glial progenitors. Science *345*, 82–87.

England, S.J., Campbell, P.C., Banerjee, S., Swanson, A.J., and Lewis, K.E. (2017). Identification and Expression Analysis of the Complete Family of Zebrafish *pkd* Genes. Front. Cell Dev. Biol. *5*, 5.

Fidelin, K., Djenoune, L., Stokes, C., Prendergast, A., Gomez, J., Baradel, A., Del Bene, F., and Wyart, C. (2015). State-Dependent Modulation of Locomotion by GABAergic Spinal Sensory Neurons. Curr. Biol. *25*, 3035–3047.

Francius, C., Harris, A., Rucchin, V., Hendricks, T.J., Stam, F.J., Barber, M., Kurek, D., Grosveld, F.G., Pierani, A., Goulding, M., and Clotman, F. (2013). Identification of multiple subsets of ventral interneurons and differential distribution along the rostrocaudal axis of the developing spinal cord. PLoS ONE *8*, e70325.

Fu, H., Qi, Y., Tan, M., Cai, J., Hu, X., Liu, Z., Jensen, J., and Qiu, M. (2003). Molecular mapping of the origin of postnatal spinal cord ependymal cells: evidence that adult ependymal cells are derived from Nkx6.1+ ventral neural progenitor cells. J. Comp. Neurol. *456*, 237–244.

Gong, S., Zheng, C., Doughty, M.L., Losos, K., Didkovsky, N., Schambra, U.B., Nowak, N.J., Joyner, A., Leblanc, G., Hatten, M.E., and Heintz, N. (2003). A gene expression atlas of the central nervous system based on bacterial artificial chromosomes. Nature *425*, 917–925.

Goulding, M. (2009). Circuits controlling vertebrate locomotion: moving in a new direction. Nat. Rev. Neurosci. *10*, 507–518.

Guillemot, F., Lo, L.C., Johnson, J.E., Auerbach, A., Anderson, D.J., and Joyner, A.L. (1993). Mammalian achaete-scute homolog 1 is required for the early development of olfactory and autonomic neurons. Cell *75*, 463–476.

Hayashi, S., and McMahon, A.P. (2002). Efficient recombination in diverse tissues by a tamoxifen-inducible form of Cre: a tool for temporally regulated gene activation/inactivation in the mouse. Dev. Biol. *244*, 305–318.

Hayashi, M., Hinckley, C.A., Driscoll, S.P., Moore, N.J., Levine, A.J., Hilde, K.L., Sharma, K., and Pfaff, S.L. (2018). Graded Arrays of Spinal and

Supraspinal V2a Interneuron Subtypes Underlie Forelimb and Hindlimb Motor Control. Neuron *97*, 869–884.e865.

Helms, A.W., Battiste, J., Henke, R.M., Nakada, Y., Simplicio, N., Guillemot, F., and Johnson, J.E. (2005). Sequential roles for Mash1 and Ngn2 in the generation of dorsal spinal cord interneurons. Development *132*, 2709–2719.

Hochstim, C., Deneen, B., Lukaszewicz, A., Zhou, Q., and Anderson, D.J. (2008). Identification of positionally distinct astrocyte subtypes whose identities are specified by a homeodomain code. Cell *133*, 510–522.

Huang, A.L., Chen, X., Hoon, M.A., Chandrashekar, J., Guo, W., Tränkner, D., Ryba, N.J., and Zuker, C.S. (2006). The cells and logic for mammalian sour taste detection. Nature *442*, 934–938.

Huang, P., Xiong, F., Megason, S.G., and Schier, A.F. (2012). Attenuation of Notch and Hedgehog signaling is required for fate specification in the spinal cord. PLoS Genet. *8*, e1002762.

Hubbard, J.M., Böhm, U.L., Prendergast, A., Tseng, P.B., Newman, M., Stokes, C., and Wyart, C. (2016). Intraspinal Sensory Neurons Provide Powerful Inhibition to Motor Circuits Ensuring Postural Control during Locomotion. Curr. Biol. *26*, 2841–2853.

Ishimaru, Y., Inada, H., Kubota, M., Zhuang, H., Tominaga, M., and Matsunami, H. (2006). Transient receptor potential family members PKD1L3 and PKD2L1 form a candidate sour taste receptor. Proc. Natl. Acad. Sci. USA *103*, 12569–12574.

Jacquet, B.V., Salinas-Mondragon, R., Liang, H., Therit, B., Buie, J.D., Dykstra, M., Campbell, K., Ostrowski, L.E., Brody, S.L., and Ghashghaei, H.T. (2009). FoxJ1-dependent gene expression is required for differentiation of radial glia into ependymal cells and a subset of astrocytes in the postnatal brain. Development *136*, 4021–4031.

Jalalvand, E., Robertson, B., Wallén, P., Hill, R.H., and Grillner, S. (2014). Laterally projecting cerebrospinal fluid-contacting cells in the lamprey spinal cord are of two distinct types. J. Comp. Neurol. *522*, 1753–1768.

Jalalvand, E., Robertson, B., Tostivint, H., Wallén, P., and Grillner, S. (2016a). The Spinal Cord Has an Intrinsic System for the Control of pH. Curr. Biol. *26*, 1346–1351.

Jalalvand, E., Robertson, B., Wallén, P., and Grillner, S. (2016b). Ciliated neurons lining the central canal sense both fluid movement and pH through ASIC3. Nat. Commun. *7*, 10002.

Jessell, T.M. (2000). Neuronal specification in the spinal cord: inductive signals and transcriptional codes. Nat. Rev. Genet. *1*, 20–29.

Karow, M., Sánchez, R., Schichor, C., Masserdotti, G., Ortega, F., Heinrich, C., Gascón, S., Khan, M.A., Lie, D.C., Dellavalle, A., et al. (2012). Reprogramming of pericyte-derived cells of the adult human brain into induced neuronal cells. Cell Stem Cell *11*, 471–476.

Kim, E.J., Ables, J.L., Dickel, L.K., Eisch, A.J., and Johnson, J.E. (2011). Ascl1 (Mash1) defines cells with long-term neurogenic potential in subgranular and subventricular zones in adult mouse brain. PLoS ONE *6*, e18472.

Kriks, S., Lanuza, G.M., Mizuguchi, R., Nakafuku, M., and Goulding, M. (2005). Gsh2 is required for the repression of Ngn1 and specification of dorsal interneuron fate in the spinal cord. Development *132*, 2991–3002.

Kútna, V., Ševc, J., Gombalová, Z., Matiašová, A., and Daxnerová, Z. (2014). Enigmatic cerebrospinal fluid-contacting neurons arise even after the termination of neurogenesis in the rat spinal cord during embryonic development and retain their immature-like characteristics until adulthood. Acta Histochem. *116*, 278–285.

Kyrousi, C., Arbi, M., Pilz, G.A., Pefani, D.E., Lalioti, M.E., Ninkovic, J., Götz, M., Lygerou, Z., and Taraviras, S. (2015). Mcidas and GemC1 are key regulators for the generation of multiciliated ependymal cells in the adult neurogenic niche. Development *142*, 3661–3674.

Lai, H.C., Seal, R.P., and Johnson, J.E. (2016). Making sense out of spinal cord somatosensory development. Development *143*, 3434–3448.

Li, S., Mo, Z., Yang, X., Price, S.M., Shen, M.M., and Xiang, M. (2004). Foxn4 controls the genesis of amacrine and horizontal cells by retinal progenitors. Neuron *43*, 795–807.

Li, S., Misra, K., Matise, M.P., and Xiang, M. (2005). Foxn4 acts synergistically with Mash1 to specify subtype identity of V2 interneurons in the spinal cord. Proc. Natl. Acad. Sci. USA *102*, 10688–10693.

Lu, Q.R., Sun, T., Zhu, Z., Ma, N., Garcia, M., Stiles, C.D., and Rowitch, D.H. (2002). Common developmental requirement for Olig function indicates a motor neuron/oligodendrocyte connection. Cell *109*, 75–86.

Madisen, L., Zwingman, T.A., Sunkin, S.M., Oh, S.W., Zariwala, H.A., Gu, H., Ng, L.L., Palmiter, R.D., Hawrylycz, M.J., Jones, A.R., et al. (2010). A robust and high-throughput Cre reporting and characterization system for the whole mouse brain. Nat. Neurosci. *13*, 133–140.

Marichal, N., García, G., Radmilovich, M., Trujillo-Cenóz, O., and Russo, R.E. (2009). Enigmatic central canal contacting cells: immature neurons in "standby mode"? J. Neurosci. *29*, 10010–10024.

Marichal, N., García, G., Radmilovich, M., Trujillo-Cenóz, O., and Russo, R.E. (2012). Spatial domains of progenitor-like cells and functional complexity of a stem cell niche in the neonatal rat spinal cord. Stem Cells *30*, 2020–2031.

McKinney, M., and McNamara, K.J. (1991). Heterochrony: The Evolution of Ontogeny (Springer US).

Meléndez-Ferro, M., Pérez-Costas, E., Villar-Cheda, B., Rodríguez-Muñoz, R., Anadón, R., and Rodicio, M.C. (2003). Ontogeny of gamma-aminobutyric acid-immunoreactive neurons in the rhombencephalon and spinal cord of the sea lamprey. J. Comp. Neurol. *464*, 17–35.

Meletis, K., Barnabé-Heider, F., Carlén, M., Evergren, E., Tomilin, N., Shupliakov, O., and Frisén, J. (2008). Spinal cord injury reveals multilineage differentiation of ependymal cells. PLoS Biol. *6*, e182.

Mizuguchi, R., Kriks, S., Cordes, R., Gossler, A., Ma, Q., and Goulding, M. (2006). Ascl1 and Gsh1/2 control inhibitory and excitatory cell fate in spinal sensory interneurons. Nat. Neurosci. *9*, 770–778.

Mori, T., Tanaka, K., Buffo, A., Wurst, W., Kühn, R., and Götz, M. (2006). Inducible gene deletion in astroglia and radial glia–a valuable tool for functional and lineage analysis. Glia *54*, 21–34.

Orts-Del'Immagine, A., Kastner, A., Tillement, V., Tardivel, C., Trouslard, J., and Wanaverbecq, N. (2014). Morphology, distribution and phenotype of polycystin kidney disease 2-like 1-positive cerebrospinal fluid contacting neurons in the brainstem of adult mice. PLoS ONE *9*, e87748.

Orts-Del'Immagine, A., Seddik, R., Tell, F., Airault, C., Er-Raoui, G., Najimi, M., Trouslard, J., and Wanaverbecq, N. (2016). A single polycystic kidney disease 2-like 1 channel opening acts as a spike generator in cerebrospinal fluid-contacting neurons of adult mouse brainstem. Neuropharmacology *101*, 549–565.

Pacary, E., Heng, J., Azzarelli, R., Riou, P., Castro, D., Lebel-Potter, M., Parras, C., Bell, D.M., Ridley, A.J., Parsons, M., and Guillemot, F. (2011). Proneural transcription factors regulate different steps of cortical neuron migration through Rnd-mediated inhibition of RhoA signaling. Neuron *69*, 1069–1084.

Park, H.C., Shin, J., and Appel, B. (2004). Spatial and temporal regulation of ventral spinal cord precursor specification by Hedgehog signaling. Development *131*, 5959–5969.

Parras, C.M., Schuurmans, C., Scardigli, R., Kim, J., Anderson, D.J., and Guillemot, F. (2002). Divergent functions of the proneural genes Mash1 and Ngn2 in the specification of neuronal subtype identity. Genes Dev. *16*, 324–338.

Pattyn, A., Simplicio, N., van Doorninck, J.H., Goridis, C., Guillemot, F., and Brunet, J.F. (2004). Ascl1/Mash1 is required for the development of central serotonergic neurons. Nat. Neurosci. *7*, 589–595.

Peng, C.Y., Yajima, H., Burns, C.E., Zon, L.I., Sisodia, S.S., Pfaff, S.L., and Sharma, K. (2007). Notch and MAML signaling drives Scl-dependent interneuron diversity in the spinal cord. Neuron *53*, 813–827.

Petracca, Y.L., Sartoretti, M.M., Di Bella, D.J., Marin-Burgin, A., Carcagno, A.L., Schinder, A.F., and Lanuza, G.M. (2016). The late and dual origin of cerebrospinal fluid-contacting neurons in the mouse spinal cord. Development *143*, 880–891.

Pogoda, H.M., von der Hardt, S., Herzog, W., Kramer, C., Schwarz, H., and Hammerschmidt, M. (2006). The proneural gene ascl1a is required for endocrine differentiation and cell survival in the zebrafish adenohypophysis. Development *133*, 1079–1089.

Raposo, A.A.S.F., Vasconcelos, F.F., Drechsel, D., Marie, C., Johnston, C., Dolle, D., Bithell, A., Gillotin, S., van den Berg, D.L.C., Ettwiller, L., et al. (2015). Ascl1 Coordinately Regulates Gene Expression and the Chromatin Landscape during Neurogenesis. Cell Rep. *10*, 1544–1556.

Rowitch, D.H., and Kriegstein, A.R. (2010). Developmental genetics of vertebrate glial-cell specification. Nature *468*, 214–222.

Shimada, I.S., Acar, M., Burgess, R.J., Zhao, Z., and Morrison, S.J. (2017). Prdm16 is required for the maintenance of neural stem cells in the postnatal forebrain and their differentiation into ependymal cells. Genes Dev. *31*, 1134–1146.

Shimizu, T., Janssens, A., Voets, T., and Nilius, B. (2009). Regulation of the murine TRPP3 channel by voltage, pH, and changes in cell volume. Pflugers Arch. *457*, 795–807.

Shin, J., Poling, J., Park, H.C., and Appel, B. (2007). Notch signaling regulates neural precursor allocation and binary neuronal fate decisions in zebrafish. Development *134*, 1911–1920.

Smith, K.K. (2003). Time's arrow: heterochrony and the evolution of development. Int. J. Dev. Biol. *47*, 613–621.

Stam, F.J., Hendricks, T.J., Zhang, J., Geiman, E.J., Francius, C., Labosky, P.A., Clotman, F., and Goulding, M. (2012). Renshaw cell interneuron specialization is controlled by a temporally restricted transcription factor program. Development *139*, 179–190.

Stoeckel, M.E., Uhl-Bronner, S., Hugel, S., Veinante, P., Klein, M.J., Mutterer, J., Freund-Mercier, M.J., and Schlichter, R. (2003). Cerebrospinal fluid-contacting neurons in the rat spinal cord, a gamma-aminobutyric acidergic system expressing the P2X2 subunit of purinergic receptors, PSA-NCAM, and GAP-43 immunoreactivities: light and electron microscopic study. J. Comp. Neurol. *457*, 159–174.

Stolt, C.C., Lommes, P., Sock, E., Chaboissier, M.C., Schedl, A., and Wegner, M. (2003). The Sox9 transcription factor determines glial fate choice in the developing spinal cord. Genes Dev. *17*, 1677–1689.

Sugimori, M., Nagao, M., Bertrand, N., Parras, C.M., Guillemot, F., and Nakafuku, M. (2007). Combinatorial actions of patterning and HLH transcription factors in the spatiotemporal control of neurogenesis and gliogenesis in the developing spinal cord. Development *134*, 1617–1629.

Suzuki, N., Ohneda, O., Minegishi, N., Nishikawa, M., Ohta, T., Takahashi, S., Engel, J.D., and Yamamoto, M. (2006). Combinatorial Gata2 and Sca1 expression defines hematopoietic stem cells in the bone marrow niche. Proc. Natl. Acad. Sci. USA *103*, 2202–2207.

Tsai, H.H., Li, H., Fuentealba, L.C., Molofsky, A.V., Taveira-Marques, R., Zhuang, H., Tenney, A., Murnen, A.T., Fancy, S.P., Merkle, F., et al. (2012). Regional astrocyte allocation regulates CNS synaptogenesis and repair. Science *337*, 358–362.

van Doorninck, J.H., van Der Wees, J., Karis, A., Goedknegt, E., Engel, J.D., Coesmans, M., Rutteman, M., Grosveld, F., and De Zeeuw, C.I. (1999). GATA-3 is involved in the development of serotonergic neurons in the caudal raphe nuclei. J. Neurosci. *19*, RC12.

Vierbuchen, T., Ostermeier, A., Pang, Z.P., Kokubu, Y., Südhof, T.C., and Wernig, M. (2010). Direct conversion of fibroblasts to functional neurons by defined factors. Nature *463*, 1035–1041.

Vígh, B., and Vigh-Teichmann, I. (1971). Structure of the medullo-spinal liquor-contacting neuronal system. Acta. Biol. Acad. Sci. Hung. *22*, 227–243.

Vígh, B., and Vigh-Teichmann, I. (1998). Actual problems of the cerebrospinal fluid-contacting neurons. Microsc. Res. Tech. *41*, 57–83.

Vígh, B., Vigh-Teichmann, I., and Aros, B. (1977). Special dendritic and axonal endings formed by the cerebrospinal fluid contacting neurons of the spinal cord. Cell Tissue Res. *183*, 541–552.

Vígh, B., Vigh-Teichmann, I., Manzano e Silva, M.J., and van den Pol, A.N. (1983). Cerebrospinal fluid-contacting neurons of the central canal and terminal ventricle in various vertebrates. Cell Tissue Res. *231*, 615–621.

Vígh, B., Manzano e Silva, M.J., Frank, C.L., Vincze, C., Czirok, S.J., Szabó, A., Lukáts, A., and Szél, A. (2004). The system of cerebrospinal fluid-contacting neurons. Its supposed role in the nonsynaptic signal transmission of the brain. Histol. Histopathol. *19*, 607–628.

Vue, T.Y., Kim, E.J., Parras, C.M., Guillemot, F., and Johnson, J.E. (2014). Ascl1 controls the number and distribution of astrocytes and oligodendrocytes in the gray matter and white matter of the spinal cord. Development *141*, 3721–3731.

Wildner, H., Müller, T., Cho, S.H., Bröhl, D., Cepko, C.L., Guillemot, F., and Birchmeier, C. (2006). dILA neurons in the dorsal spinal cord are the product of terminal and non-terminal asymmetric progenitor cell divisions, and require Mash1 for their development. Development *133*, 2105–2113.

Yang, L., Rastegar, S., and Strähle, U. (2010). Regulatory interactions specifying Kolmer-Agduhr interneurons. Development *137*, 2713–2722.

Yeo, S.Y., and Chitnis, A.B. (2007). Jagged-mediated Notch signaling maintains proliferating neural progenitors and regulates cell diversity in the ventral spinal cord. Proc. Natl. Acad. Sci. USA *104*, 5913–5918.

Yu, K., McGlynn, S., and Matise, M.P. (2013). Floor plate-derived sonic hedgehog regulates glial and ependymal cell fates in the developing spinal cord. Development *140*, 1594–1604.

Zhou, Q., and Anderson, D.J. (2002). The bHLH transcription factors OLIG2 and OLIG1 couple neuronal and glial subtype specification. Cell *109*, 61–73.

STAR★METHODS

KEY RESOURCES TABLE

REAGENT or RESOURCE	SOURCE	IDENTIFIER
Antibodies		
Mouse Anti-Nkx2.2	DSHB	Cat# 74.5A5; RRID: AB_531794
Mouse Anti-Nkx6.1	DSHB	Cat# F55A10; RRID: AB_532378
Mouse Anti-Pax6	DSHB	Cat# Pax6; RRID: AB_528427
Mouse Anti-Lhx3	DSHB	Cat# 67.4E12; RRID: AB_2135805
Mouse Anti-Isl1/2	DSHB	Cat# 40.2D6; RRID: AB_528315
Mouse Anti-Ascl1	BD Pharmigen	Cat# 556604; RRID: AB_396479
Rabbit Anti-Ascl1	Babco	N/A
Guinea pig Anti-Gata2	Peng et al., 2007	N/A
Mouse Anti-Gata3	Santa Cruz	Cat# SC-268; RRID: AB_2108591
Rabbit Anti-PKD2L1	Huang et al., 2006	N/A
Goat Anti-Sox2	Santa Cruz	Cat# SC-17320; RRID: AB_2286684
Goat Anti-Sox9	R&D Systems	Cat# AF3075; RRID: AB_2194160
Mouse Anti-βIII-tubulin	Covance	Cat# MMS435P; RRID: AB_2313773
Rabbit Anti-Hb9	Sam Pfaff, Salk Institute, CA, USA.	N/A
Rabbit Anti-Olig2	Chemicon	Cat#AB9610; RRID: AB_570666
Mouse Anti-FoxA2	Abcam	Cat# ab117542; RRID: AB_10938341
Rabbit Anti-EGFP	Molecular Probes	Cat# A11122; RRID: AB_221569
Chicken Anti-EGFP	Aves Laboratories	Cat# GFP-1020; RRID: AB_10000240
Rabbit Anti-dsRed	Clontech	Cat# 632496; RRID: AB_10013483
Guinea pig Anti-Chx10	Sam Pfaff, Salk Institute, CA, USA.	N/A
Rat Anti-βGal	Martyn Goulding, Salk Institute, CA, USA	N/A
Rat Anti-Pax3	Martyn Goulding, Salk Institute, CA, USA	N/A
Rat Anti-BrdU	Immunodirect	Cat# MCA2060T; RRID: AB_566394
Rabbit Anti-Nfia	Active motif	Cat#39397; RRID: AB_2314931
Chicken Anti-Vimentin	Chemicon	Cat# AB5733; RRID: AB_11212377
Mouse Anti-S100β	Sigma	Cat# S2532; RRID: AB_477499
Mouse Anti-NeuN	Chemicon	Cat# A60; RRID: AB_2314889
Mouse Anti-Foxj1	eBioscience	Cat#14-9965-80; RRID: AB_1548836
Secondary antibodies	Jackson ImmunoResearch Laboratories (West Grove, PA)	N/A
Experimental Models: Organisms/Strains		
Ascl1^{Neo}	Guillemot et al., 1993	MGI ID: 1857470
Ascl1^{CreERT2}	Kim et al., 2011	MGI ID: 4452601
Ascl1^{flox}	Pacary et al., 2011	MGI ID: 5141455
Tg Ascl1:GFP	Gong et al., 2003	MGI ID: 3845062
Ascl1^{KiNgn2}	Parras et al., 2002	MGI ID: 2388165
Gata2^{GFP}	Suzuki et al., 2006	MGI ID: 2673268
Foxn4^{LacZ}	Li et al., 2004	MGI ID: 3054789
Tg CAG:CreER	Hayashi and McMahon, 2002	MGI ID: 2182767
Glast^{CreERT2}	Mori et al., 2006	MGI ID: 3830051
Gata3^{LacZ}	van Doorninck et al., 1999	MGI ID: 2181200
Ai14 td-Tomato	Madisen et al., 2010	MGI ID: 3809524
pia^{t25215}	Pogoda et al., 2006	ZFIN ZDB-ALT-040716-18

(*Continued on next page*)

Continued

REAGENT or RESOURCE	SOURCE	IDENTIFIER
Oligonucleotides		
See Table S1 for primers used in this study		N/A
Morpholino: MO-Ascl1b TCGTAGCGACGACAGTTGCCTCCAT	Gene Tools LLC	ZFIN ZDB-MRPHLNO-050308-14
Software and Algorithms		
Photoshop	Adobe	N/A
Illustrator	Adobe	N/A
Prism Graphpad	Graphpad Software	N/A
MATLAB	Mathworks	N/A
Zeiss LSM Image Browser	Zeiss	N/A

LEAD CONTACT AND MATERIALS AVAILABILITY

Further information and requests for resources and reagents should be directed to and will be fulfilled by the Lead Contact, Guillermo Lanuza (glanuza@leloir.org.ar). This study did not generate new unique reagents.

EXPERIMENTAL MODEL AND SUBJECT DETAILS

Mice

All experiments were conducted according to the protocols approved by the Institutional Animal Care and Use Committee (IACUC) of Fundación Instituto Leloir. Mouse lines used: *Ascl1*^{neo} (Guillemot et al., 1993), *Ascl1*^{CreER} (Kim et al., 2011), *Ascl1*^{neoflox} (Pacary et al., 2011), *Ascl1:GFP* (AU176, Gensat; Gong et al., 2003), *Ascl1*^{Neurog2} (Parras et al., 2002), *Gata2*^{GFP} (Suzuki et al., 2006), *Foxn4* (Li et al., 2004), *CAG:CreER* (Hayashi and McMahon, 2002), *Gata3*^{lacZ} (van Doorninck et al., 1999), *Glast*^{CreER} (Mori et al., 2006) and *Ai14 td-Tomato* conditional reporter (Madisen et al., 2010). Mice were housed under controlled environment in a 12h light/dark cycle, with food and water *ad libitum*. Time pregnancies were determined by detection of vaginal plug and midday was designated embryonic day (E) 0.5. Control animals were wild-type (wt) littermates or offsprings with genotypes without phenotypic effects. Gender was not determined. Genotyping of mice was performed by PCR using allele-specific primers (see Table S1).

Zebrafish

Zebrafish experiments were done in accordance to the national animal welfare committees (LANUV Nordrhein-Westfalen) and the University of Cologne. Zebrafish line used: *pia*^{t25215} *ascl1a* mutant (Pogoda et al., 2006). Experiments were performed in 24 hpf (hours post-fertilization) embryos; gender was not determined.

METHOD DETAILS

Animals

Induction of CreER activity was achieved by tamoxifen (Tam) administration at the indicated stages. Dosis of Tam were 75 mg/kg b.w. i.p. or 3 pulses of 50 mg/kg for *Ascl1*^{CreER}, 150 mg/kg for *CAG:CreER* and 5 mg/kg for *Glast*^{CreER}. Embryos were dissected in PBS buffer. Embryos or isolated cords were fixed for 1 h in 4% paraformaldehyde (PFA in PBS) and cryoprotected in 20% sucrose (overnight, 4°C) prior to embedding in Cryoplast (Biopack). Stage-matched littermates of desired genotypes were aligned and embedded together to ensure identical processing conditions. Tissue was cryosectioned 30 μm thick (Leica 3050S, Leica Biosystems).

Zebrafish *pia*^{t25215} mutants, which have a truncated version of *ascl1a*, were identified by the absence of lactotropes, assessed by *in situ* hybridization against prl (Pogoda et al., 2006). The antisense morpholino (MO) for *ascl1b* (5′-TCGTAGCGACGACA GTTGCCTCCAT-3′, Gene Tools LLC) was diluted in 1x Danieu's buffer at 0.033 pmol/nl and injected (1-1.5 nl) into embryos at the one- to four-cell stage.

Immunohistochemistry

Antibody stainings were performed as previously described (Carcagno et al., 2014). Briefly, cryostat sections were washed in PBS containing 0.1% Tween20 (PBST) and treated with blocking solution (5% HI-serum, 0.1% Triton X-100 in PBS) for 1h. Primary antibodies at the appropriate dilutions in blocking solution were incubated overnight at 4°C. After incubation, slides were washed 3 times 10 min each with PBST and incubated with Cy-labeled species-specific secondary antibodies (Jackson ImmunoResearch) for 2-3 h. at RT. Sections were mounted with PVA-DABCO or dehydrated in ethanol/xylene series and mounted with DPX (Sigma Aldrich). For antibody details, see "Key Resources Table."

In BrdU-labeling experiments, females were injected with bromodeoxyuridine (i.p. 20-50 mg/kg b.w. for multiple or single administrations, respectively). Previous to immunohistochemistry, HCl-antigen retrieval was performed.

In situ hybridization

Non-radioactive *in situ* hybridization in mouse sections was performed as previously described (Carcagno et al., 2014). Briefly, tissue sections were fixed 15 min with PFA 4%, treated with proteinase K (3 μg/ml, 3 min), followed by PFA 4% 10 min and PBS washes. Slides were incubated in triethanolamine-acetic anhydrate pH 8.0 10 min, permeabilized with Triton X-100 1% in PBS for 30 min and washed. Sections were incubated for 2 h with hybridization solution (50% formamide, 5x SSC, 5x Denhardt, 250 μg/ml yeast tRNA). Digoxigenin-labeled RNA probes were generated by *in vitro* transcription. Probes used were Pkd1l2 (Petracca et al., 2016), Gata2 and Ascl1 (Carcagno et al., 2014). Slides were blocked with 10% HI-serum in TBS 0.1% tween-20 for 2 h, incubated O.N. at 4°C with alkaline phosphatase-labeled anti-DIG antibody (Roche) and enzymatic activity was detected with BCIP and NBT. In zebrafish embryos, single and double whole-mount *in situ* hybridizations were performed as described previously (Pogoda et al., 2006). Riboprobes used were *pkd2l1* (this study) and *prl* (prolactin) to recognize *ascl1a* mutants (Pogoda et al., 2006). Brightfield pictures were captured by digital camera on Zeiss Axioplan microscope.

Acute Spinal Cord Slice Recordings

Tissue isolation and recording were done as described before (Petracca et al., 2016). E18.5 Spinal cords were dissected in chilled low-Calcium Ringer's solution (in mM: 128 NaCl, 4.69 KCl, 25 $NaHCO_3$, 1.18 KH_2PO_4, 3.25 $MgSO_4$, 0.25 $CaCl_2$, 1.3 $MgCl_2$ and 22 glucose, saturated with 5% CO_2-95% O_2). Slices (400 μm thick) were cut in vibrating microtome (Leica VY1000E) and transferred to artificial CSF (in mM: 125 NaCl, 2.5 KCl, 2 NaH_2PO_4, 25 $NaHCO_3$, 2 $CaCl_2$, 1.3 $MgCl_2$, 1.3 Na-ascorbate, 3.1 Na-pyruvate, 10 dextrose; 315 mOsm) bubbled with 95% O_2-5% CO_2 at 30°C for > 1h. Following recovery, slices were transferred to a recording chamber mounted on an Olympus BX61WI microscope at RT.

Tomato$^+$ cells around the central canal were identified by fluorescence and infrared DIC videomicroscopy using an EM-CCD camera (Hamamatsu). Whole-cell recordings were performed using microelectrodes (4-5MΩ) filled with (mM): 150 K-gluconate, 4 $MgCl_2$, 0.1 EGTA, 1 NaCl, 10 HEPES, 4 ATP-tris, 0.3 GTP-tris, 10 phosphocreatine. All recordings were obtained using Axopatch 200B amplifiers, digitized and acquired at 20 KHz using pClamp 10 (Molecular Devices). Input resistance was obtained from current traces evoked by a hyperpolarizing step of 10 mV. Voltage-dependent currents were recorded by applying conditioning voltage steps of 10 mV from −60 mV holding potential. Spiking responses were recorded by applying depolarizing current steps (5 pA increments; 500 ms) under current clamp, keeping the cells at −60 mV. To subtract leakage currents, we used the P/N subtraction protocol in pClamp 10. Dye-coupled cells were visualized in living slices by injecting LuciferYellow-CH (0,1%, Molecular Probes) through the patch pipette.

Imaging

Images were captured using Zeiss LSM 510 Meta and Zeiss LSM5 Pascal confocal microscopes using LSM Image Browser Software (Zeiss). Micrographs were processed using Adobe Photoshop and Adobe Illustrator.

QUANTIFICATION AND STATISTICAL ANALYSIS

At least ten sections were examined from each embryo, and no less than three embryos of each genotype were used. In all experiments, control animals from the same litter were used. Results are shown as mean ± SD, unless stated. Differences between groups were evaluated by non-parametric Mann-Whitney U test, Kruskal-Wallis one-way analysis of variance with post hoc Dunn's Multiple Comparison test or Fisher test (GraphPad Software Inc). Results were considered statistically significant when $p < 0.05$ (*$p < 0.05$, **$p < 0,01$, ***$p < 0.001$). Ascl1 levels were assessed using a MATLAB script (Carcagno et al., 2014) to measure intensity of individual cells. A cell was considered Ascl1^{HIGH} when its intensity was above 4 SD of background.

DATA AND CODE AVAILABILITY

The published article includes all datasets/codes generated or analyzed during this study.

Cell Reports, Volume *28*

Supplemental Information

Ascl1 Balances Neuronal versus Ependymal Fate in the Spinal Cord Central Canal

Daniela J. Di Bella, Abel L. Carcagno, M. Lucía Bartolomeu, M. Belén Pardi, Heiko Löhr, Nicole Siegel, Matthias Hammerschmidt, Antonia Marín-Burgin, and Guillermo M. Lanuza

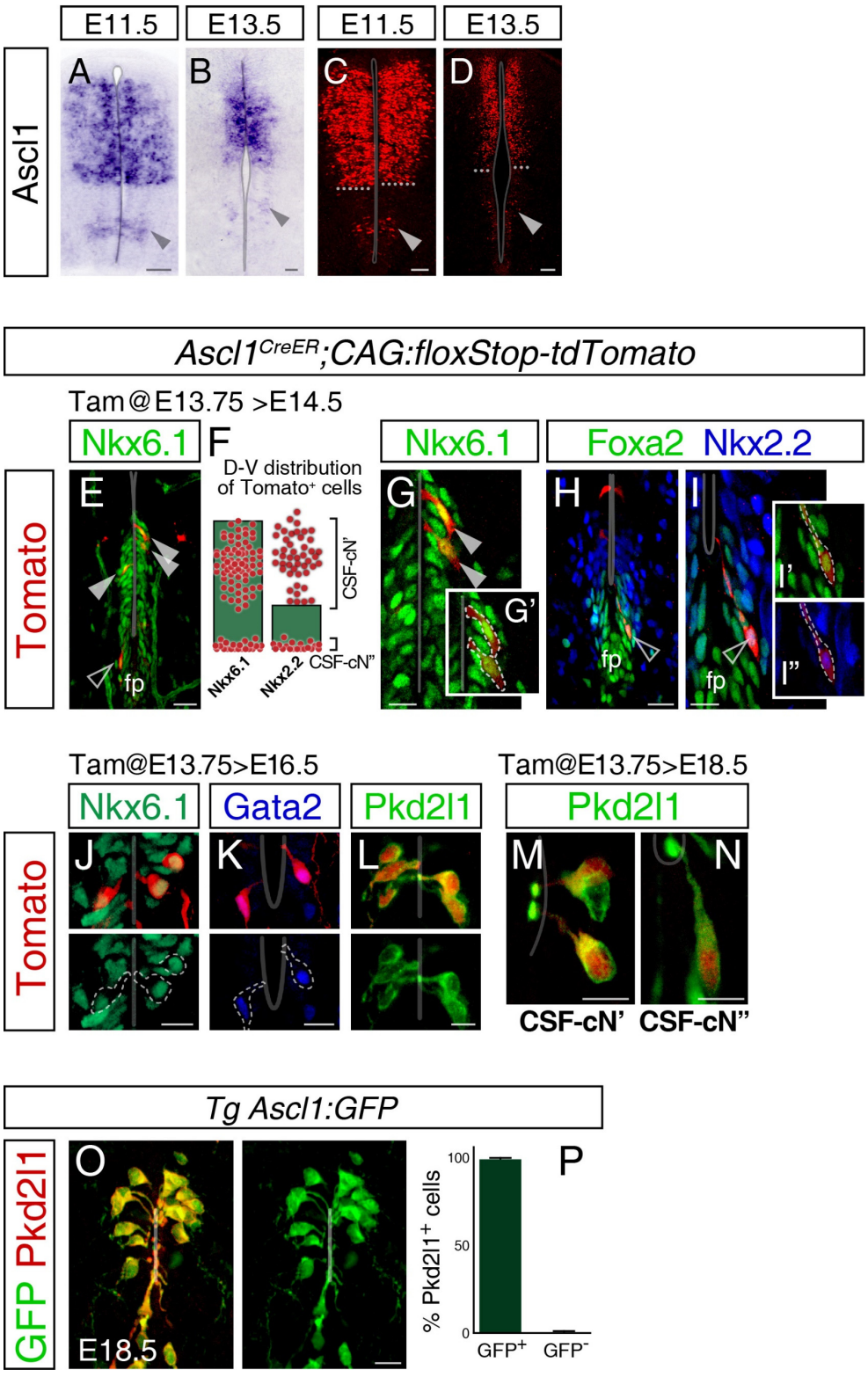

Figure S1. Related to Figure 1.

Ascl1 ventral spinal cord progenitors give rise to cerebrospinal fluid-contacting neurons.

A-D) Ascl1 expression in the developing spinal cord. *In situ* hybridizations (**A-B**) and immunohistochemistry (**C-D**) for Ascl1 on E11.5 and E13.5 spinal cord cross sections. Ascl1 is expressed in the dorsal ventricular zone and in a limited number of ventral cells (arrowheads). Dashed lines indicate the ventral limit of the dorsal domain.

E-N) Late Ascl1^{+} progenitors give rise to both CSF-cN' and CSF-cN''. *Ascl1^{CreER};CAG:floxStop-tdTomato* embryos were treated with tamoxifen at E13.75 (75mg/kg i.p.) and analyzed at E14.5 (**E-I**), E16.5 (**J-L**) or E18.5 (**M-N**). Detection of Tomato at E14.5 together with Nkx6.1 (**E,G**) or Foxa2 and Nkx2.2 (**H-I**) identified cells in the p2/pOL domain (**E,G**, filled arrowheads, CSF-cN') and p3 adjacent to the floor plate (**E,H,I**, empty arrowheads, CSF-cN"). **F)** Dorso-ventral position of Tomato^{+} cells (n=161, 4 embryos) analyzed together with Nkx6.1 or Nkx2.2 indicate that Ascl1-derived cells are clustered similarly to CSF-cN' and CSF-cN" subsets (Petracca et al., 2016). Green bars indicate the dorso-ventral extension of Nkx6.1 and Nkx2.2. **J-L)** E16.5 Tomato^{+} cells with the characteristic morphology of CSF-cN stained against Nkx6.1 (**J**), Gata2 (**K**) or Pkd2l1 (**L**). **M-N)** Magnification of Ascl1-derived CSF-cNs at E18.5, stained for Tomato and Pkd2l1. Tomato is selectively expressed in Pkd2l1^{+} cells in the lateral aspects of the central canal (CSF-cN', **M**) and ventral to the central canal (CSF-cN", **N**).

O-P) All CSF-cN derive from Ascl1^{+} cells. Short-term lineage tracing in the *Ascl1:GFP* transgenic line. Perinatal spinal cord sections stained against Pkd2l1 and GFP. All CSF-cNs were GFP^{+} (n=337/337 cells analyzed, 2 embryos).

Bars are mean±SD. Scale bars are 50µm in A-D, 20µm in E,H,O and 10µm in G,I,J-N.

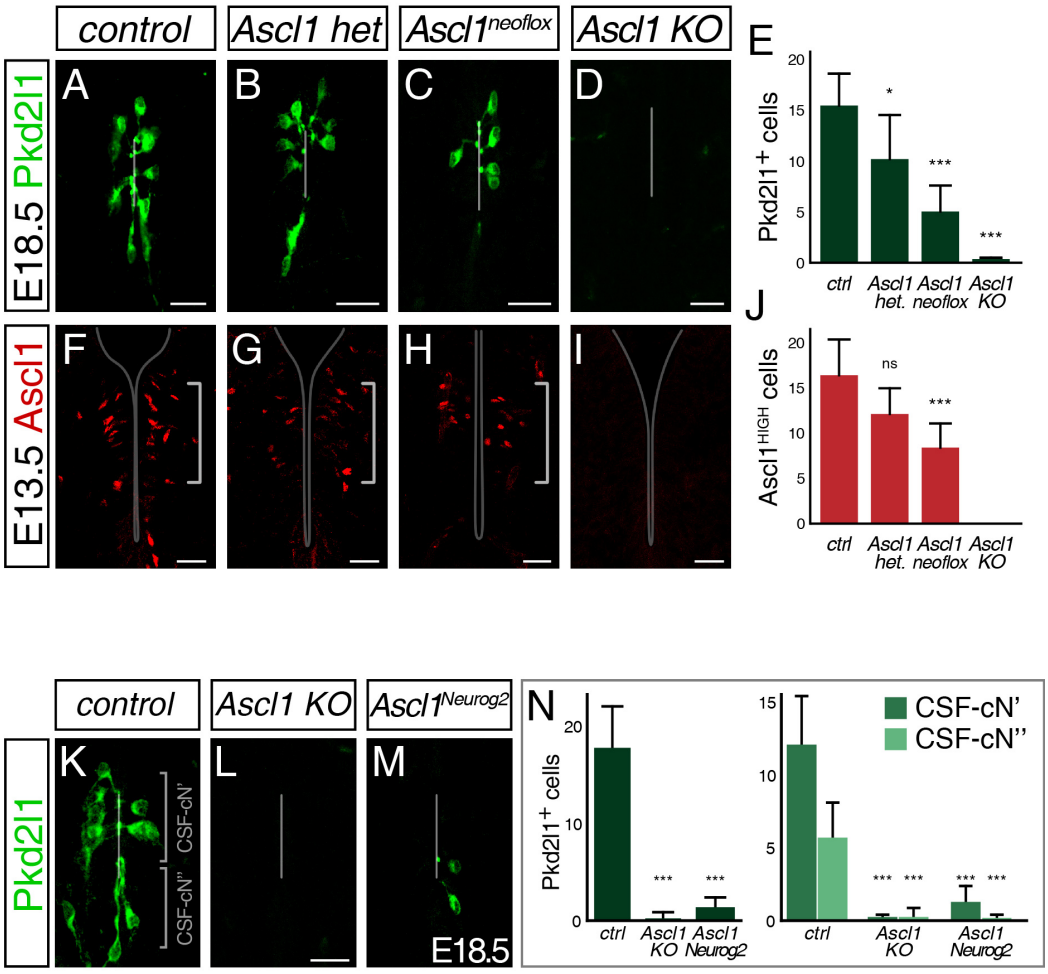

Figure S2. Related to Figure 2.
Ascl1 controls CSF-cN differentiation.

A-J) CSF-cN differentiation depends on Ascl1 expression levels. Cross sections of E18.5 spinal central canal (**A-D**) and E13.5 ventral neural tube (**F-I**) of *control* (**A,F**), *Ascl1*$^{+/-}$ (heterozygous, **B,G**), hypomorphic *Ascl1*^{neoflox} (**C,H**) and *Ascl1*$^{-/-}$ (**D,I**) mice, stained with antibodies against Pkd2l1 (**A-D**) or Ascl1 (**F-I**). Quantifications of Pkd2l1^{+} cells per section (**E,** n=18-30 sections, 2-4 embryos each) and Ascl1^{HIGH} cells per hemisection (**J,** n=6-20 sections, 1-2 embryos each) show correlation between the number of Ascl1^{+} cells at E13.5 and Pkd2l1^{+} neurons at E18.5. Quantification in E includes data in Figure 2D.

K-N) Ascl1 is specifically required for CSF-cN differentiation. E18.5 spinal cord sections immunostained against Pkd2l1 in *control* (**K**), *Ascl1 KO* (**L**) or homozygous *Ascl1*^{Neurog2} (**M**) mice. The quantification of total Pkd2l1^{+} neurons, CSF-cN' and CSF-cN'' per section (**N**) indicates that Neurog2 cannot replace Ascl1 function (n=30-40 sections, 2-4 embryos each).

Bars are mean±SD. ***p<0.001; *p<0.05; ns, non-significant; Kruskal-Wallis test followed by Dunn's multiple comparison test. Scale bars are 20µm.

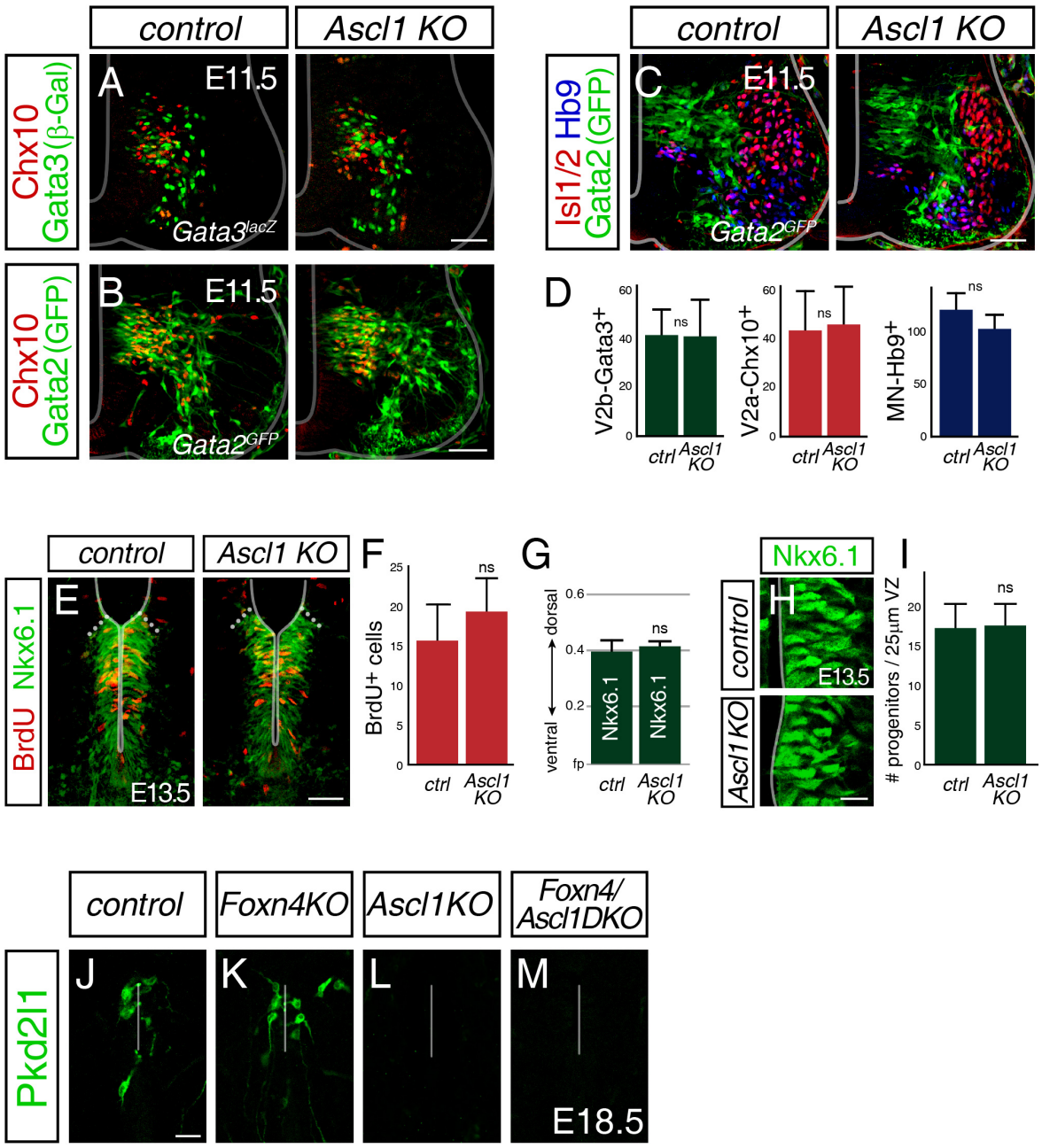

Figure S3. Related to Figure 3.
Ascl1 controls the late neurogenesis in the mammalian spinal cord.

A-D) Lack of Ascl1 does not affect early neurogenesis in the ventral neural tube. E11.5 spinal cord sections of *control* and *Ascl1 KO* mice stained against Chx10 and Gata3 (**A**, β-Gal in *Gata3*^{lacZ}), Chx10 and Gata2 (**B**, GFP in *Gata2*^{GFP}), and Hb9, Isl1/2 and GFP (**C**). The numbers of Gata2/3^{+} V2b interneurons, Chx10^{+} V2a interneurons or Hb9^{+} motoneurons (**D**) were not significantly changed in *Ascl1 KO* E11.5 (n=5-10 sections, 1-2 embryos each), or other stages (not shown).

E-I) Ventricular zone patterning and proliferation is normal in *Ascl1* mutants. E13.5 spinal cord sections from control and *Ascl1 KO* mice 3hs after BrdU administration (50mg/kg i.p.), stained for

Nkx6.1 and BrdU (**E**). The number of $BrdU^+$ cells per hemisection is unchanged (**F**), as well as the dorso-ventral extension of the Nkx6.1 (**G**, dotted lines in **E**). **H)** Magnifications of $Nkx6.1^+$ cells in the ventricular zone of *control* and *Ascl1 KO* mice. The density of $Nkx6.1^+$ progenitors (expressed per 25µm ventricular opening) is similar between genotypes (**I**). (n=4-10 sections, 1-2 embryos each)

J-M) Ascl1 controls CSF-cN development also in the absence of Foxn4. Pkd2l1-expressing neurons in E18.5 spinal cord of *control* (**J**), *Foxn4 KO* (**K**), *Ascl1 KO* (**L**) and *Foxn4;Ascl1 double KO (DKO*, **M***)*. In absence of Foxn4, Ascl1 is still required for CSF-cN development.

Bars are mean±SD. ns, non-significant, Mann-Whitney test. Scale bars are 40µm in A-C,E, 10µm in H and 20µm in J-M.

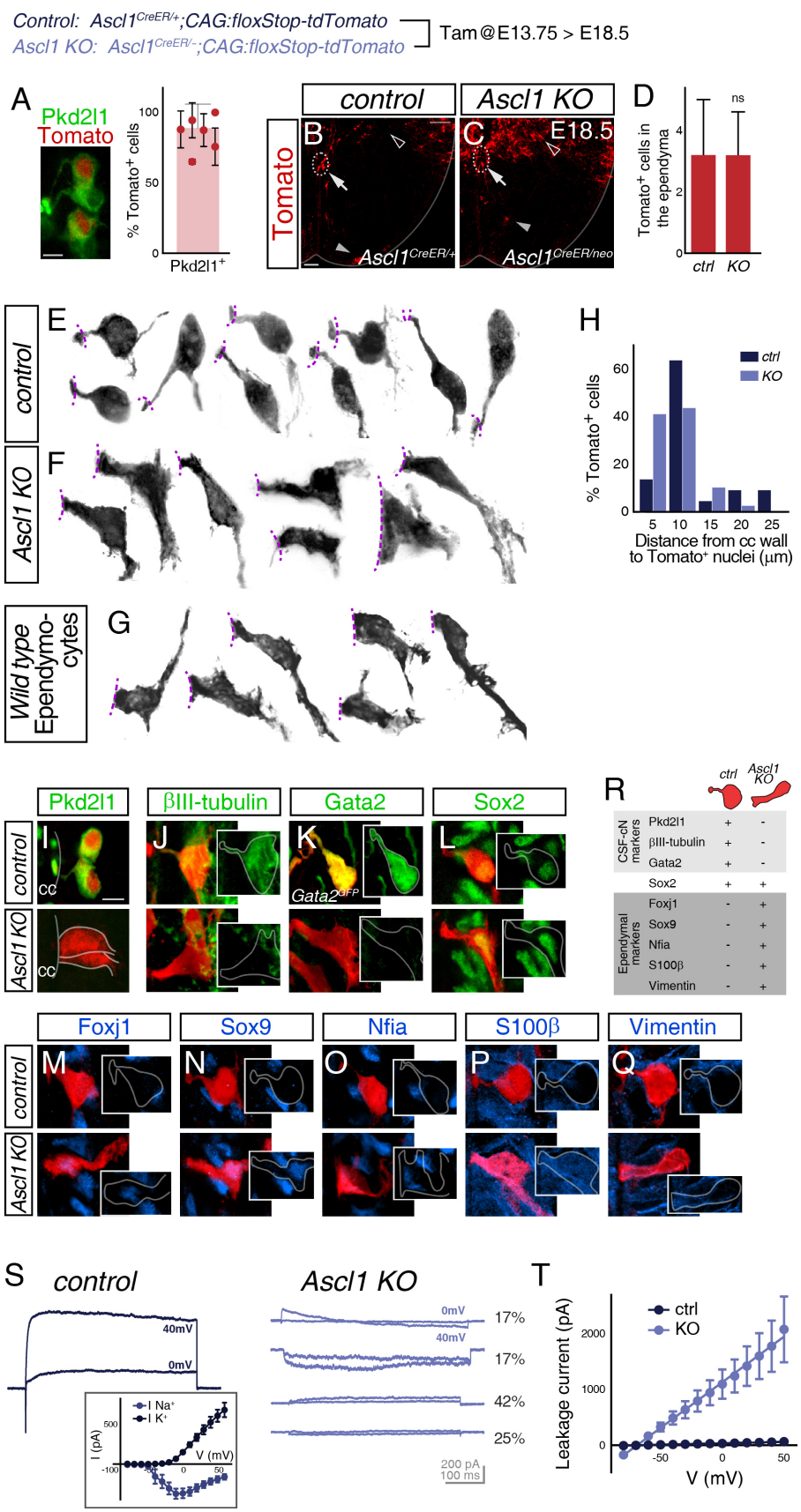
Control: Ascl1CreER/+;CAG:floxStop-tdTomato
Ascl1 KO: Ascl1CreER/-;CAG:floxStop-tdTomato
Tam@E13.75 > E18.5
A
Pkd2l1
Tomato
% Tomato+ cells
Pkd2l1+
control
Ascl1 KO
B
C
E18.5
Tomato
Ascl1CreER/+
Ascl1CreER/neo
D
ns
Tomato+ cells in the ependyma
ctrl
KO
E
F
G
control
Ascl1 KO
Wild type Ependymo-cytes
H
ctrl
KO
% Tomato+ cells
Distance from cc wall to Tomato+ nuclei (µm)
Pkd2l1
βIII-tubulin
Gata2
Sox2
I
J
K
L
cc
Gata2GFP
R
ctrl
Ascl1 KO
CSF-cN markers
Pkd2l1 + -
βIII-tubulin + -
Gata2 + -
Sox2 + +
Ependymal markers
Foxj1 - +
Sox9 - +
Nfia - +
S100β - +
Vimentin - +
Foxj1
Sox9
Nfia
S100β
Vimentin
M
N
O
P
Q
S
control
40mV
0mV
I Na+
I K+
I (pA)
V (mV)
Ascl1 KO
0mV
40mV
17%
17%
42%
25%
200 pA
100 ms
T
ctrl
KO
Leakage current (pA)
V (mV)

Figure S4. Related to Figure 4
Ascl1 regulates ependymal *vs.* neuronal fate decision in the late spinal cord

A-D) *Ascl1*^{CreER} faithfully identifies prospective CSF-cN progenitors. E18.5 spinal cord of *Ascl1*$^{CreER/+}$*;CAG:floxStop-tdTomato* (*control*) and *Ascl1*$^{CreER/-}$*;CAG:floxStop-tdTomato* (*Ascl1 KO*), in which recombination was induced by a single dose of tamoxifen at E13.75. This protocol labeled CSF-cNs as shown by Tomato expression in Pkd2l1$^+$ cells. The percentage of Tomato$^+$ cells around the central canal that expressed Pkd2l1 in *control* mice ranged between 74-100% in different experiments (**A**). Ascl1-derived cells comprise dorsal astrocytes (**B**, empty arrowhead), CSF-cN around the central canal (**B**, arrow) and few ventral glial cells (**B**, filled arrowhead). In the absence of Ascl1, an increased number of labeled dorsal astrocytes were found (C, empty arrowhead, Vue et al.,2014), but without changes in ventral cells in the parenchyma (**C**, filled arrowhead) or in the ependymal zone (**B,C**, arrow). Quantification of the number of Tomato$^+$ cells in the area of the central canal shows no difference between *control* and *mutant* mice (**D**, n=10-20 sections, 3 embryos each). Bars are mean±SD. ns, non-significant; Mann-Whitney test.

E-G) Examples of cellular morphologies found in *control* animals and *mutants*. The central canal (cc) is located on the left (dashed purple lines). In *control* spinal cords, Tomato$^+$ cells display the appearance of CSF-cNs, with its distinctive process contacting the CSF. In the *Ascl1 mutants*, although displaying some morphological heterogeneity (**F**), they are part of the ventricular surface, with a wider apical contact and no protruding processes. The basal cellular extensions are extensively branched and thicker than in *controls*. **G)** Examples showing morphological heterogeneity of central canal ependymocytes at E18.5 labeled with *Glast*^{CreER}*;CAG:floxStop-tdTomato* (low dose of TAM, E12.5). **H)** Distribution analysis of the distance of the cell nuclei to the surface of the cc shows that Tomato$^+$ cells in *mutant*s tend to occupy positions closer to the cc, while in *control* mice, labeled CSF-cN are mostly subependymal (n=40-60 cells each).

I-R) Prospective CSF-cN progenitors express ependymocyte markers in the absence of Ascl1. E18.5 spinal cord sections of *Ascl1*$^{CreER/+}$*;CAG:floxStop-tdTomato* (*control*) and *Ascl1*$^{CreER/-}$*;CAG:floxStop-tdTomato* (*Ascl1 KO*) induced with tamoxifen at E13.75, stained for the CSF-cN identity markers: Pkd2l1 (**I**), βIII-tubulin (**J**), Gata2 (**K**, GFP, *Gata2*^{GFP}) or Sox2 (**L**), and the ependymocyte markers Foxj1 (**M**), Sox9 (**N**), Nfia (**O**), S100β (**P**) and Vimentin (**Q**). Sox2 labels both CSF-cNs and ependymocytes. In the *controls*, labeled cells express CSF-cN markers, while in *Ascl1 KO* mice they only express ependymal proteins (summarized in **R**).

S-T) Electrophysiological recordings of labeled cells in *control* and *Ascl1 KO* acute slices. Whole cell voltage clamp recordings of currents evoked with depolarizing pulses (0mV, 40mV, 500ms, n=11-13 cells). Inset: current-voltage plot of the peak inward fast and steady-state outward current in *control* mice. In *Ascl1 KO*s, Tomato$^+$ cells exhibited the diverse responses described for ependymocytes. The percentages of cells matching each electrophysiological profile is indicated to the right. **T)** I-V graph of the leakage currents determined in Tomato-labeled cells in *control* and *Ascl1 mutant* spinal cords. Tomato$^+$ cells in the mutants exhibit robust leakage currents as described for mural ependymal cells. Data is mean±SEM.

Scale bars are 5μm, except 40μm in B,C.

Table S1. Oligonucleotides used for genotyping in this study. Related to STAR Methods and Key Resources Table

oligo name	oligo sequence	source
NeoF1	GCATACGCTTGATCCGGCTACC	this paper
NeoR1	AAGGCGATGCGCTGCGAATC	this paper
EGFP1	GACGTAAACGGCCACAAGTT	this paper
EGFP2	GAACTCCAGCAGGACCATGT	this paper
td-Tomato Fw	ACGGCATGGACGAGCTGTAC	this paper
td-Tomato Rev	CAGGCGAGCAGCCAAGGCAA	this paper
Cre3-Rv	TAATCGCCATCTTCCAGCAG	this paper
CreJ-Fw	GCGGTCTGGCAGTAAAAACTATC	this paper
Foxn4-1	GGCCTCTCTGTCCATACCTGTA	this paper
Foxn4-2	CTACTCTCTTTGATGACAGCTCCC	this paper
lacz392	TTGGCGTAAGTGAAGCGAC	this paper
lacz393	AGCGGCTGATGTTGAACTG	this paper
Ascl1wt1	CTCCGGGAGCATGTCCCCAA	this paper
Ascl1wt2	CCAGGACTCAATACGCAGGG	this paper
Ascl1fl wtFw	CTACTGTCCAAACGCAAAGTGG	this paper
Ascl1fl wtRev	GCTCCCACAATCCTCGTAAAGA	this paper
Ascl1fl Rev	TAGACGTTGTGGCTGTTGTAGT	this paper